

Chapter 5

Computational Studies of Thermal Transport Properties of Carbon Nanotube Materials

Leonid V. Zhigilei, Richard N. Salaway, Bernard K. Wittmaack,
and Alexey N. Volkov

5.1 Introduction

Carbon nanotube (CNT) materials constitute a broad class of hierarchical materials deriving their properties from the intimate connections between the atomic structure of individual CNTs, the arrangements of CNTs into mesoscopic structural elements, such as CNT bundles and branching structures, and the structural organization of the mesoscopic elements into macroscopic network materials. Depending on the material density and production method, the CNT materials exist in many forms, from low-density aerogels and sponges with densities of $\sim 0.01 \text{ g/cm}^3$ [1, 2], to medium-density CNT films [3–6], “forests” [7, 8], mats, and “buckypaper” [9–11] with densities of $\sim 0.1 \text{ g/cm}^3$, and to high-density super-aligned CNT fibers [12–14], forests [8] and films [15] with CNT arrangements approaching the ideal packing limit. While, in general, the strong van der Waals attraction between nanotubes [16] results in their self-assembly into networks of interconnected bundles [17, 18], the degree of CNT alignment, bundle and pore size distributions, and other structural characteristics of CNT networks are not uniquely defined by the length and flexural rigidity of CNTs and material density, but can be modulated by changing the

L.V. Zhigilei (✉) • B.K. Wittmaack
Department of Materials Science and Engineering, University of Virginia, 395 McCormick Road,
Charlottesville, VA 22904-4745, USA
e-mail: lz2n@virginia.edu

R.N. Salaway
Department of Mechanical and Aerospace Engineering, University of Virginia, 122 Engineers
Way, Charlottesville, VA 22904-4746, USA

A.N. Volkov
Department of Mechanical Engineering, University of Alabama, 7th Avenue,
Tuscaloosa, AL 35407, USA

parameters of the production process [18], mechanical [11] and chemical [19, 20] post-processing or radiative treatment.

The complex hierarchical organization of the CNT materials and the wide diversity of material structures give rise to a large variability of physical properties. The experimentally measured values of thermal conductivity of CNT materials, in particular, fall into an amazingly broad range of values from 0.02 to 1000 W/m/K [14, 15, 21–34] and suggest that the variation in structure and density of the CNT networks as well as the modulation of the intrinsic thermal conductivity of individual CNTs can turn CNT materials from perfect thermal conductors to insulators. Moreover, the high degree of anisotropy of thermal conductivity reported for aligned arrays of nanotubes [24, 26, 30] opens up attractive opportunities for guiding the heat transport along a desired path in thermal management applications. In order to realize these opportunities, however, a clear understanding of the key microstructural features and elementary processes that control thermal transport properties of CNT materials has to be achieved.

As reviewed in Chap. 10 of this book, the steady advancement in experimental techniques for probing thermal conductivity of individual CNTs and CNT materials has yielded important information on the connections between the structural characteristics of CNT materials and their thermal transport properties. The small size of the individual nanotubes and their propensity to form bundles and aggregate into intertwined structures, however, present a number of technical challenges that hamper a systematic experimental investigation of the dependence of thermal conductivity on the geometrical and structural parameters of CNTs (length, diameter, chirality, strain, and presence of defects) and their arrangement into network structures. The experimental challenges have motivated extensive computational efforts aimed at providing insights into the mechanisms and pathways of the heat transfer in CNT materials.

Due to the complexity and inherently multiscale nature of the structural organization of the CNT network materials, a complete analysis of the heat transfer cannot be performed within a single computational approach and a number of complementary computational techniques have to be combined for establishing the connections between the intrinsic thermal conductivity of individual CNTs, intertube thermal conductance, and the collective heat transfer through the CNT material, as schematically shown in Fig. 5.1. The atomistic molecular dynamics (MD) computational technique is well suited for simulation of the vibrational (phononic) heat transfer in individual CNTs [35–69] or heat exchange between CNTs [21, 70–81]. The information gained from the atomistic simulations can be used for parameterization of mesoscopic models that adopt simplified representations of nanotubes and are capable of simulating the collective behavior and properties of large ensembles of CNTs arranged into interconnected networks of bundles [82–99]. A detailed analysis of the results of the mesoscopic simulations of heat flow in CNT materials with realistic entangled structures [60, 79, 100, 101] can provide ideas for designing theoretical models of the heat (and charge) transfer in CNT materials and, in particular, for making a transition from the theoretical analysis of model systems composed of straight randomly arranged or aligned nanofibers

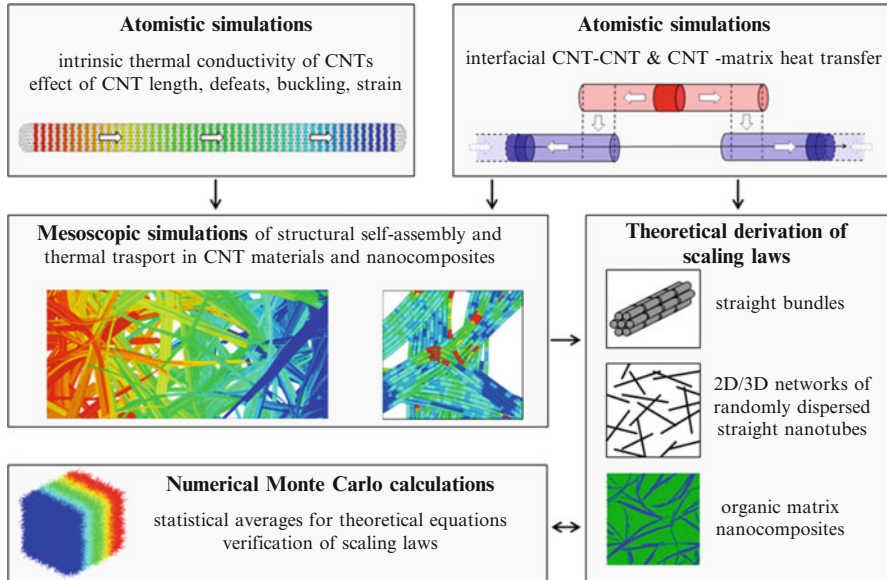


Fig. 5.1 Schematic diagram of the connections between different computational approaches aimed at providing insights into the heat transfer in CNT materials and advancing theoretical understanding of thermal transport properties of this practically important class of nanofibrous network materials

[72, 100–114] to the derivation of the scaling laws for complex network structures and nanocomposites. The statistically averaged thermal transport properties of CNT networks can be obtained with a number of theoretical approaches based on simplified geometrical models of fibrous networks or numerically in Monte Carlo simulations [100, 102–105, 109, 110, 112–114]. These theoretical and numerical approaches provide additional guidance for revealing the scaling laws that govern the structure–properties relationships of the transport properties of CNT materials. Overall, the atomistic and mesoscopic modeling plays an important role in the advancement of the theoretical understanding of the heat transfer in CNT materials and, in general, in a broad class of network nanofibrous materials.

In this chapter, we first provide a brief overview of the results of atomistic simulation studies of the thermal conductivity of individual CNTs and inter-tube contact conductance (Sects. 5.2 and 5.3), and then discuss the emerging mesoscopic computational approaches to the calculation of the effective thermal conductivity of CNT materials (Sects. 5.4 and 5.5). The interconnections between the processes occurring at different length scales are highlighted and the open questions and future research directions are discussed in Sect. 5.6.

5.2 Atomistic Modeling of Thermal Conductivity of Individual CNTs

The classical MD technique has been (and remains) the most commonly used computational method in investigations of heat transfer in CNT systems. The MD technique allows one to follow the time evolution in a system of interacting atoms by solving a set of classical equations of motion for all atoms in the system [115]. A key advantage of this technique is in its ability to fully control the conditions of the simulations and to perform systematic analysis of the dependence of the thermal conductivity on CNT length [38–41, 44–50, 54, 55, 62–68], diameter [37–39, 44, 47–49, 54, 57, 59, 62–65], elastic deformation [51–53, 58, 67], buckling [51, 56, 60, 61, 67], presence of isotope dopants [44, 45, 49, 64], vacancies and Stone–Wales defects [36, 45, 64], or chemisorbed molecules [40] in a systematic manner and in isolation from other structural parameters. Despite the full control over the simulated system, however, the MD simulation technique can hardly be considered to be suitable for quantitative predictions of the exact values of thermal conductivity of CNTs. The two main limiting factors, the classical treatment of atomic motions and the sensitivity of the results to the computational parameters, are briefly described below.

Since the Debye temperature of CNTs is on the order of 1000 K, the phonon population at room temperature is governed by quantum mechanics (Bose–Einstein statistics), and cannot be adequately represented by the classical MD technique. Quantum corrections, based on redefining the temperature so that the classical kinetic energy of the system is equal to the corresponding quantum kinetic energy of a harmonic lattice, have been developed for the description of thermodynamic and structural properties [116, 117] and extended to thermal transport properties in a number of works, e.g., [46, 50]. This extension, however, has been shown to be flawed [118] as the classical and quantum relaxation times cannot be reconciled using a system-level quantum correction. A number of more refined “quantum thermal bath” approaches accounting for quantum-mechanical effects through application of a Langevin-type thermostat with a colored noise enforcing the Bose–Einstein distribution of the vibrational energy have recently been suggested [118–123]. The complexity of these approaches as well as a number of technical issues, such as the zero-point energy leakage [124, 125], however, restricts their applications to relatively simple model systems, and leaves the challenge of fully accounting for quantum effects in MD simulations unresolved.

Beyond the missing quantum effects, the predictive power of MD simulations is affected by the sensitivity of the results to the computational procedures and interatomic potentials employed in the calculations. Even when the simulated system is nominally the same, the values of thermal conductivity predicted in different MD simulations exhibit a surprisingly large variability. An example of such inconsistency is demonstrated by the sample of MD results obtained for single-walled (10, 10) CNTs at ~ 300 K provided in Table 5.1. The values of thermal conductivity range from $\sim 100 \text{ Wm}^{-1} \text{ K}^{-1}$ to more than $6000 \text{ Wm}^{-1} \text{ K}^{-1}$, and are

Table 5.1 A sample of room temperature values of CNT thermal conductivity, k_T , predicted in MD simulations of (10,10) CNTs performed with equilibrium MD (EMD) method, where k_T is calculated from small fluctuations of heat current using Green–Kubo relation [115], non-equilibrium MD (NEMD) method, where a steady-state temperature gradient is created between “heat bath” regions and k_T is determined from the Fourier law, and homogenous NEMD (HNEMD) method [126], in which k_T is evaluated from the response of the system to a small artificial “thermal force” applied to individual atoms and representing the effects of the heat flow

Source	k_T ($\text{Wm}^{-1} \text{K}^{-1}$)	L_T (nm)	Potential	Method	Boundary conditions
Lukes and Zhong [46]	~20–160	5–40	Brenner-2 + LJ	EMD	Periodic and non-periodic
Ma et al. [67]	~105–175	~25–90	AIREBO	NEMD	Periodic
Pan [57]	243	~29.4	Brenner-2	NEMD	Periodic
Salaway and Zhigilei [66]	154–258	47–630	AIREBO	NEMD	Non-periodic
Xu and Buehler [51]	301	49.26	AIREBO	NEMD	Periodic
Wei et al. [58]	302	49.26	AIREBO	NEMD	Periodic
Padgett and Brenner [40]	~35–350	~10–310	Brenner-2	NEMD	Periodic
Thomas et al. [54]	~300–365	200–1000	Brenner-2	NEMD	Non-periodic
Lukes and Zhong [46]	233–375	5–10	Brenner-2 + LJ	HNEMD	Periodic
Maruyama [38]	~275–390	6–404	Brenner	NEMD	Non-periodic
Feng et al. [64]	~50–590	6.52–35	Brenner-2	NEMD	Non-periodic
Bi et al. [45]	~400–600	2.5–25	Tersoff	EMD	Periodic
Moreland et al. [41]	215–831	50–1000	Brenner	NEMD	Periodic
Cao and Qu [62]	~560–1620	100–2400	Tersoff-2	NEMD	Periodic
Ren et al. [53]	~1430	6	AIREBO	NEMD	Non-periodic
Sääskilahti et al. [68]	~160–1600	~120–4000	Tersoff-2	NEMD	Non-periodic
Grujicic et al. [42]	1730–1790	~2.5–40	AIREBO	EMD	Periodic
Che et al. [36]	~2400–3050	~2.5–40	Brenner	EMD	Periodic
Berber et al. [35]	~6600	~2.5	Tersoff	HNEMD	Periodic

The definition of the length of the CNTs, L_T , includes the length of the heat bath regions [66]. The interatomic potentials used in the simulations are the Tersoff potential in its original formulation [127, 128] (Tersoff) and with parameters suggested in [129] (Tersoff-2), the Brenner potentials with parameterizations described in [130, 131] (Brenner and Brenner-2, respectively), and the adaptive intermolecular reactive bond order (AIREBO) potential described in [132]. A description of non-bonding van der Waals interactions through addition of the Lennard-Jones (LJ) potential to the Brenner-2 potential is denoted as Brenner-2 + LJ

clearly affected by the computational setups adopted in different studies. A recent analysis of the effects of common computational parameters of non-equilibrium MD simulations [66] demonstrates that the type of boundary conditions, size and location of heat bath regions, definition of the CNT length, and the choice of interatomic potential all have a substantial influence on the predicted values of thermal conductivity. The choice of interatomic potential, in particular, is shown to be responsible for an up to fourfold variability in thermal conductivity for otherwise identical simulation conditions.

While the above discussion casts doubt on the utility of MD simulations for evaluation of accurate values of thermal conductivity of CNTs, the real power of the MD simulations is in the ability to reveal the general trends and physical mechanisms that control the heat transfer within and between the nanotubes, as well as to provide a valuable semi-quantitative information on the effect of different factors (e.g., CNT length, structural defects, and different modes of deformation) on thermal conductivity of CNTs.

The length dependence of thermal conductivity of CNTs, in particular, is commonly observed in MD simulations [33, 36, 38–44, 46–49, 54, 61, 63–68] and attributed to two main physical origins. First, when the length of a nanotube is smaller than or comparable to the phonon mean free path, phonons are capable of traveling ballistically through the CNT without being impeded by phonon–phonon scattering. As the CNT length increases, the effective length of the ballistic transport increases, which also increases the overall thermal transport and results in higher conductivity values. Second, the longest available phonon wavelength that can exist in a CNT is defined by the length of the nanotube. Thus, as the length increases, the maximum allowable phonon wavelength also increases. The additional long-wavelength phonons offer effective channels for thermal transport and can make a substantial contribution to the thermal conductivity [46, 62, 67, 68].

The CNT length that corresponds to the transition from the ballistic heat conduction regime, where the thermal conductivity increases with CNT length, to the diffusive regime, where the thermal conductivity approaches a constant value, is temperature dependent as the phonon mean free path decreases with increasing temperature. A recent review of room temperature experimental measurements performed for CNTs with length exceeding 0.5 μm [33] suggests the diffusive regime of the heat transfer. At the same time, the results of MD simulations performed for CNTs with lengths of 10–100s of nm typically exhibit a pronounced increase of k_T with increasing CNT length, that is the characteristic of the ballistic phonon transport [38–41, 44, 46–49, 54, 62, 64, 66, 68]. The length dependences predicted in different MD studies, however, vary widely for the same (10,10) CNT, with the transition to the diffusive regime (saturation of k_T) predicted for as short CNTs as 100 nm or even in some of the investigations [36, 42, 43, 63], while no saturation is observed for CNTs with length exceeding 1 μm in other studies [62, 68].

A sample set of computational results shown in Fig. 5.2 suggests the dominant contribution from the ballistic phonon transport for CNTs shorter than ~ 200 nm,

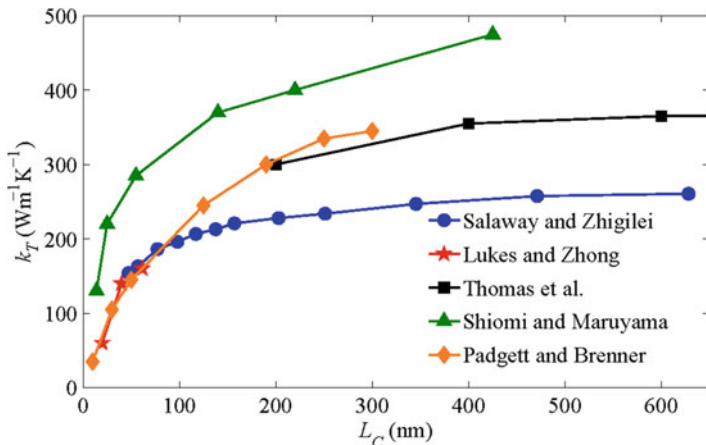


Fig. 5.2 Dependences of thermal conductivity, k_T , of (10,10) CNTs on sample length, L_C , predicted in MD simulations by Lukes and Zhong [46], Thomas et al. [54], Shiomi and Maruyama [48], Padgett and Brenner [40], and Salaway and Zhigilei [66]. The sample length is defined as the distance between the hot and cold heat bath regions

which exhibit strong length dependence. In studies where CNTs longer than 200 nm are investigated, a transition to weaker length dependence is observed, suggesting a transition to the diffusive-ballistic regime. The transition between the two regimes is observed for the nanotube length that roughly corresponds to the room temperature phonon mean free path, which has been estimated to be of the order of 200–500 nm based on experimental data [133, 134], results of MD simulations [62], and theoretical analysis [135]. Note that the extent of the transitional diffusive-ballistic regime is defined by the longest mean free paths of long-wavelength phonons (of the order of several μm [136] or even longer [68] at room temperature). Thus, while the length dependences shown in Fig. 5.2 become notably weaker as the length increases above 200 nm, the gradual increase of the thermal conductivity with increasing length may be expected up to CNT lengths of the order of tens of μm [68, 137, 138].

While the computational studies discussed above are addressing the intrinsic thermal conductivity of perfect fully relaxed CNTs, the nanotubes in a real material are likely to contain various structural defects and experience elastic deformation caused by their interaction with surrounding CNTs in an interconnected network of bundles or application of an external mechanical loading to the material. The precise control over atomic structure and strain in MD simulations makes it possible to perform a detailed analysis of the effect of mechanical deformation and defects on thermal conductivity of CNTs.

In particular, the effect of the axial deformation was investigated in non-equilibrium MD (NEMD) simulations reported in [51] and a substantial reduction of the thermal conductivity for both tension ($\sim 30\%$ reduction for strain of 15%, close

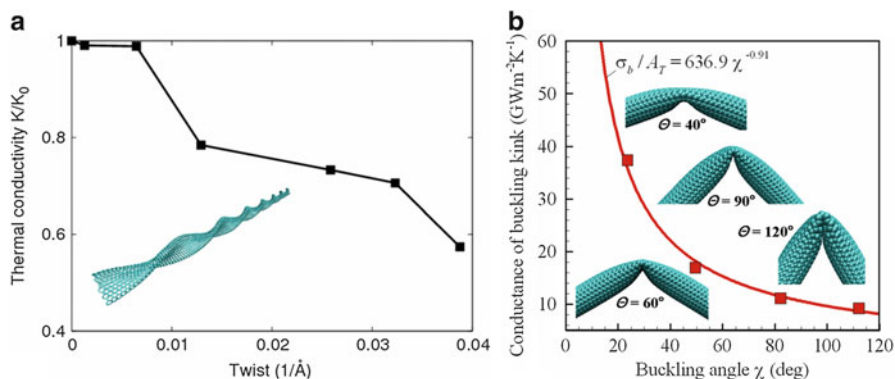


Fig. 5.3 The dependences of the nanotube thermal conductivity on torsional deformation [51] (a) and thermal conductance of bending buckling kink normalized by the cross-sectional area of a CNT, σ_b/A_T , on the buckling angle χ [60] (b) predicted for (10,10) CNTs in MD simulations. The insets show atomic configurations for a twist strain of 0.026 in (a) and for buckling angles $\chi = 23.6^\circ$, 49.5° , 82.1° , and 112.0° (correspond to bending angles $\theta = 40^\circ$, 60° , 90° , and 120° , respectively) in (b)

to the failure limit) and compression (up to $\sim 36\%$ reduction for strain of -5%) was observed for a 49 nm long (10,10) CNT. The reduction of thermal conductivity was attributed to softening of phonon modes under tension and enhanced phonon scattering due to the transverse bending/buckling upon compression. In another study, performed for a shorter, 6 nm long (10,10) CNT [53], the maximum of thermal conductivity was observed at about 2% elongation of the nanotube while additional elongation and compression are found to decrease the conductivity. The torsional strain is reported to have a negligible effect on thermal conductivity up to the onset of buckling of the nanotube cross-section, when the thermal conductivity exhibits a substantial drop, Fig. 5.3a [51]. A similar behavior is observed for bending deformation, where the effect of bending on thermal conductivity is hardly noticeable [52, 67] up to the onset of bending buckling, while the appearance of buckling kinks creates effective “thermal resistors” for the heat conduction along the nanotube [51, 60, 61, 67]. The results of MD simulations performed for different bending angles reveal a strong dependence of the thermal conductance of a buckling kink on the buckling angle, Fig. 5.3b [60], and enable reliable parameterization of a mesoscopic model capable of simulating heat transfer in network structures composed of thousands of CNTs (see Sect. 5.4). The mesoscopic simulations show that the effect of the finite buckling conductance is amplified by the preferential buckling of thin bundles and individual CNTs serving as interconnections between thicker bundles in the network structures, resulting in about 20% reduction in the effective conductivity of a network material composed of 1 μm long (10,10) CNTs [60].

Overall, the results of the MD simulations of strained nanotubes suggest that homogeneous elastic deformation of nanotubes has relatively small effect on their

thermal conductivity, while the onset of geometric instability and buckling greatly enhances scattering of phonons and decreases thermal conductivity. This conclusion is also consistent with the results of recent simulations of the free vibrations of 26 nm long (10,10) CNTs, where a dramatic increase in the rate of the energy dissipation of longitudinal and bending oscillations (i.e., the energy transfer from low-frequency mechanical oscillations to high-frequency vibrational modes) is observed at the onset of axial or bending buckling [90].

5.3 Atomistic Modeling of Inter-Tube Contact Conductance

Despite the high intrinsic thermal conductivity of individual CNTs, the values of the effective conductivity reported for CNT-based materials are often relatively low and exhibit large variability [14, 15, 21–34]. The weak thermal coupling between CNTs, defined by non-bonding van der Waals inter-tube interactions, is commonly assumed to be the limiting factor that controls thermal transport in CNT materials [21, 70–77, 100, 139–141]. This assumption has been put into question by the results of recent mesoscopic simulations [101], which suggest that the effective thermal conductivity of CNT network materials is to a large extent controlled by the finite values of the intrinsic thermal conductivity of the nanotubes (see Sect. 5.4). Nevertheless, the dependence of the inter-tube conductance on the density and geometrical characteristics of the CNT–CNT contacts is clearly critical for establishing the physical mechanisms of heat transfer in CNT materials.

The only direct experimental measurements of thermal conductance between individual nanotubes reported to date are the ones reported in [140, 141] for multi-walled CNTs. The results of these measurements indicate that the conductance per unit area is about an order of magnitude lower for CNTs that are aligned with each other at the contact as compared to the CNTs crossing each other at an angle [140]. The strong dependence of the interfacial conductance on the geometry of the contact suggests a high sensitivity of the effective thermal conductivity of CNT materials to their structural organization and puts into question the reliability of the estimations of the inter-tube contact conductance based on the experimental values of the effective conductivity of CNT materials [21, 34, 113, 144]. These estimations typically assume a fixed value of the inter-tube conductance and rely on analytical equations derived for idealized systems composed of randomly dispersed straight nanotubes [72, 100, 101, 111]. The arrangement of CNTs into bundles in real CNT materials, however, can result in a broad spectrum of the inter-tube contacts, which has been shown to have a dramatic effect on the inter-tube heat exchange and the effective thermal conductivity [100, 101].

Under conditions when nanoscale manipulation of CNTs and reliable measurement of the conductance between individual nanotubes still present significant challenges, computational analysis based on MD simulations has been playing the leading role in advancing the physical understanding of the thermal transport across CNT–CNT contacts [21, 70–81]. The simulations have provided important

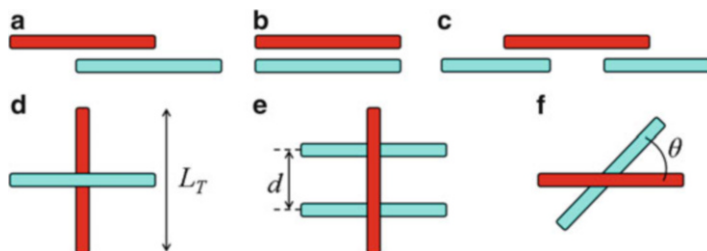


Fig. 5.4 Schematic representations of computational setups used in MD simulation studies of the inter-tube contact conductance: (a–c) parallel, partially or fully overlapping CNTs and (d–f) CNTs crossing each other at an angle. The setup in (e), with two cross-junctions separated by a distance d , is used for investigation of the effect of contact density on the conductance per junction

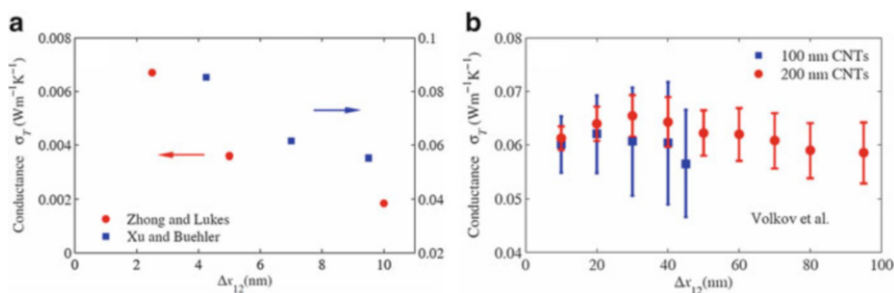


Fig. 5.5 Inter-tube conductance per unit length, σ_T , versus overlap length, Δx_{12} , predicted in MD simulations of parallel partially overlapping (10,10) CNTs by Zhong and Lukes [70], Xu and Buehler [74] (a), and Volkov et al. [79] (b). The computational setup of Fig. 5.4a with rigid boundary conditions applied to the outer ends of the two nanotubes is used by Zhong and Lukes, while the setup shown in Fig. 5.4c with periodic boundary conditions applied in the direction parallel to the axes of nanotubes is used in the other two studies. The *error bars* in (b) show one sample standard deviation calculated for “instantaneous” values of inter-tube conductance collected during the steady-state part of the simulation

insights into the mechanisms responsible for the inter-tube heat transfer for parallel CNTs [70, 71, 74, 75, 77, 79, 81] and CNTs crossing each other at an angle [21, 72, 73, 76–78, 80, 81]. Various configurations used in MD simulations of inter-tube conductance are schematically represented in Fig. 5.4. Similarly to the MD simulations of the intrinsic conductivity of CNTs discussed above, in Sect. 5.2, quantitative comparison of the values of inter-tube conductance predicted in different simulations is hampered by the differences in computational setups, interatomic potentials, definitions of the contact area, and length and type of the CNTs used in the simulations. Nevertheless, it may be instructive to compare the results obtained in different investigations of the well-studied (10,10) CNTs that are also used as an example in the discussion of CNT conductivity in the previous section.

Starting with parallel, partially overlapping CNTs (setups shown in Fig. 5.4a, c) and plotting the data reported in [70, 74, 79] in a uniform way, in terms of conductance per overlap length, σ_T in units of $\text{Wm}^{-1} \text{K}^{-1}$, in Fig. 5.5, two trends can be observed. In the simulations performed for short overlap length, $\Delta x_{12} \leq 10$ nm, the conductance per overlap length is decreasing with increasing overlap length [70, 74]. The drop in σ_T is particularly sharp in simulations reported in [70], from $\sigma_T \approx 0.0065 \text{ Wm}^{-1} \text{K}^{-1}$ at $\Delta x_{12} = 2.5$ nm, to $\sigma_T \approx 0.0034 \text{ Wm}^{-1} \text{K}^{-1}$ at $\Delta x_{12} = 5$ nm, and to $\sigma_T \approx 0.0018 \text{ Wm}^{-1} \text{K}^{-1}$ at $\Delta x_{12} = 10$ nm, and more moderate in simulations of [74] where σ_T decreases from ~ 0.08 to $\sim 0.05 \text{ Wm}^{-1} \text{K}^{-1}$ as Δx_{12} increases from 4 to 9.5 nm. For longer overlap lengths of 10–95 nm considered in [79], however, no statistically significant variation of σ_T with the overlap length is observed. Since the area of a CNT–CNT contact is directly proportional to the overlap length, the disparate trends observed for short and long overlaps suggest that the inter-tube contact conductance is not a simple function of the contact area and may depend on particular geometry/types of the contact.

At quantitative level, the values of σ_T obtained for long overlaps in [79], $\sim 0.06 \text{ Wm}^{-1} \text{K}^{-1}$, are consistent with the range of $0.05\text{--}0.08 \text{ Wm}^{-1} \text{K}^{-1}$ reported for shorter overlaps in [74]. Comparable values, 0.03 and $0.048 \text{ Wm}^{-1} \text{K}^{-1}$, can be calculated from the results reported for two parallel 20 nm long (10,10) CNTs [77] and two parallel 4.3 nm long (10,0) CNTs embedded into a “frozen” matrix [75],¹ respectively. On the other hand, an order of magnitude smaller values of $0.0065\text{--}0.0018 \text{ Wm}^{-1} \text{K}^{-1}$ are calculated from the data of [70]. The use of relatively short nanotubes ($L_T = 5\text{--}40$ nm as compared to $L_T = 100\text{--}200$ nm in [79] and $L_T = 25\text{--}75$ nm in [74]) in combination with fixed boundary conditions at the ends of the interacting CNTs may be responsible for both the strong overlap length dependence of σ_T and the small values of the conductance observed in [70]. Indeed, the dependence on the CNT length in [70] is especially pronounced for $L_T < 10$ nm and becomes weaker as the CNT length increases from 10 to 40 nm. The observation of the pronounced CNT length dependence for short CNTs is consistent with the results of an MD simulation study of the interfacial conductance between a (5,5) CNT and a surrounding octane liquid [139], where an increase in the interfacial conductance per CNT surface area with increasing nanotube length is observed up to a length of ~ 3.5 nm and attributed to the extinction of low-frequency phonons in short CNTs.

Further insights into the dependence of the inter-tube conductance on the contact area and the geometry of the contact can be obtained from simulations performed for CNTs crossing each other at various angles (computational setups shown in Fig. 5.4d, f). The definition of the contact area for cross-junctions, however, is not straightforward and different approaches have been adopted in different studies. In particular, the inverse thermal conductance calculated in [77] for different angles

¹The values of interface conductance given in [75] in units of $\text{Wm}^{-1} \text{K}^{-1}$ (Figs. 6 and 7 of [75]) are about an order of magnitude larger than the actual values found in the simulations, as established through private communication with Dr. Vikas Varshney.

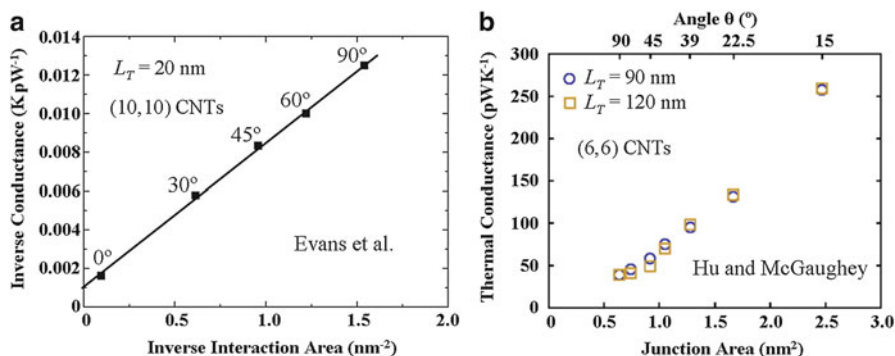


Fig. 5.6 Thermal conductance of CNT–CNT cross-junctions predicted in MD simulations by Evans et al. [77] (a) and Hu and McGaughey [80] (b). The computational setups of Fig. 5.4d, f with periodic boundary conditions applied in the direction parallel to the axes of nanotubes is used by Evans et al., while the ends of the nanotubes are kept rigid during the simulations by Hu and McGaughey. The contact area is defined through the inter-tube interaction energy in (a) and calculated as $D^2/\sin\theta$, where D is the nanotube diameter in (b)

θ is plotted in Fig. 5.6a as a function of the inverse contact area using the total inter-tube bonding energy as a measure of the contact area. The linear scaling of the inverse conductance with inverse “contact area” is discussed in this study in terms of a combined contribution of two thermal resistances placed in series, an internal resistance associated with the energy exchange between high- and low-frequency modes within the nanotubes and an external junction resistance associated with heat flow between the nanotubes mostly via low-frequency vibrational modes. The notion of the major contribution of long-wavelength phonons in the energy transfer between the nanotubes is supported by the results of wavelet analysis of thermal pulse propagation along a CNT forming perpendicular cross-junction with another nanotube [73]. Evaluation of the vibrational frequencies excited in the second CNT reveals the dominant frequencies that are relatively low (<10 THz), implying that the low-frequency modes are largely responsible for the heat transfer across CNT–CNT junctions.

An approximate linear scaling of the cross-junction conductance on the contact area is also observed in a study performed for (6,6) CNTs [80], where a simple geometrical definition of the contact area as $D^2/\sin(\theta)$, where D is the nanotube diameter, is used, Fig. 5.6b. A substantial deviation from the linear dependence, however, can be seen for the data point calculated for the smallest angle of $\theta = 15^\circ$, where deformation of the contact geometry by the inter-tube interaction forces acting to align the nanotubes may be expected.

The combined results of several series of MD simulations performed for various inter-tube contact configurations shown in Fig. 5.4 have recently been used to formulate a general model of CNT–CNT conductance applicable to junctions of arbitrary configuration [81]. The analysis of the combined set of data reveals a non-linear dependence of the conductance on the number of interatomic inter-tube

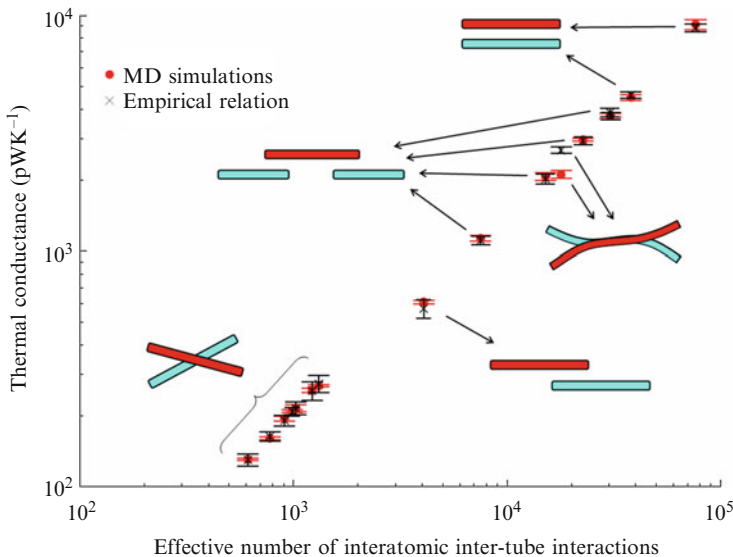


Fig. 5.7 The values of inter-tube thermal conductance obtained in MD simulations (*red circles*) and predicted by the general empirical equation (*black crosses*) for various CNT–CNT contact configurations [81]

interactions (used as a proxy for contact area) and suggests a larger contribution to the conductance from areas of the contact where the density of interatomic inter-tube interactions is smaller. An empirical relation expressing the conductance of an arbitrary contact configuration through the area of the contact region, quantified by the number of interatomic inter-tube interactions, and the density of interatomic inter-tube interactions, characterized by the average number of interatomic inter-tube interactions per atom in the contact region, is suggested based on the results of MD simulations. The empirical relation is found to provide a good quantitative description of the contact conductance for various CNT configurations, as shown in Fig. 5.7. Moreover, the empirical relation and the underlying concept of the sensitivity of the conductance to the density of interatomic inter-tube interactions reconcile the results of earlier studies of the conductance between parallel partially overlapping CNT, Fig. 5.5, where the conductance per overlap length was shown to be independent of the overlap length for long overlaps [79] but was found to exhibit a pronounced decrease with increasing length of the overlap for short overlaps [70, 74]. The general description of the conductance of an arbitrary CNT–CNT contact configuration is also suitable for incorporation into mesoscopic models capable of predicting the effective thermal transport properties of CNT network materials, as discussed below in Sect. 5.4.

Before starting the discussion of the mesoscopic modeling, we would like to mention two issues related to the inter-tube interactions in CNT materials that received a substantial, and somewhat controversial, attention in literature. First,

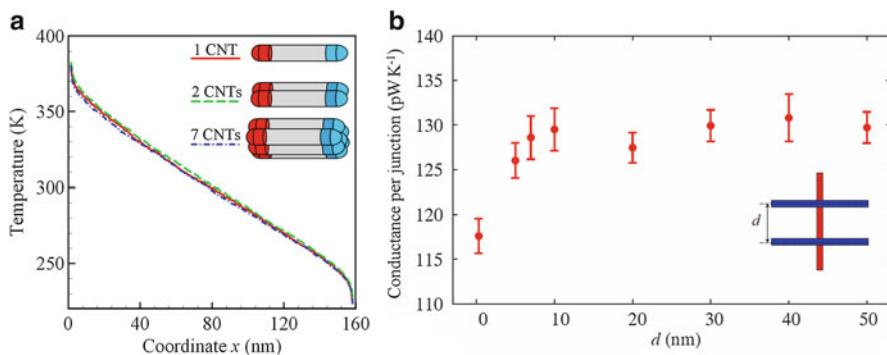


Fig. 5.8 The temperature profiles along nanotubes obtained in MD simulations performed for 160 nm long (10,10) CNTs arranged into three configurations shown in the inset [79] (a) and the values of the contact conductance predicted in simulations of double junctions separated by distance d [81] (b). In (a), the heat flux is applied to each CNT individually and the values of thermal conductivity are obtained from the steady-state temperature profiles

the van der Waals interactions between nanotubes in CNT bundles leading to the enhancement of phonon scattering and decrease in the intrinsic thermal conductivity of nanotubes is commonly discussed as a major factor responsible for a substantially lower thermal conductivity of CNT bundles as compared to individual CNTs [25, 31, 142, 143, 145]. The reduction of the intrinsic thermal conductivity of CNTs and other carbon structures due to the non-bonding interactions in materials that consist of multiple structural elements was suggested in [35] based on the results of atomistic Green-Kubo calculations of thermal conductivity. This suggestion, however, while echoed in a number of works, e.g., [31, 25, 143, 145, 146], is only a conjecture extrapolated from the computational prediction on the difference between the thermal conductivity of a graphene monolayer and graphite. An opposite conclusion of a weak effect of the interactions of perfect CNTs in a bundle on thermal conductivity, which can be substantially enhanced by structural defects, has been made in [149] based on the kinetic model calculations of thermal conductivity. To clarify the question on the effect of the inter-tube coupling in CNT bundles on the intrinsic thermal conductivity of the CNTs, a series of MD simulations was performed in [79] for systems of one, two, and seven 160 and 300 nm long (10,10) CNTs arranged in configurations shown as insets in Fig. 5.8a. The temperature profiles predicted in constant heat flux NEMD simulations for the three configurations are almost identical, Fig. 5.8a, suggesting that the thermal conductivities of individual CNTs, defined by the Fourier law, are not significantly affected by the interactions among the CNTs. Indeed, the values of k_T calculated for CNTs in each of the three configurations coincide with each other within the statistical error of the calculation.

The absence of any significant effect of the van der Waals inter-tube coupling in CNT bundles on the intrinsic thermal conductivity of individual CNTs is consistent with relatively small changes of the vibrational spectra of CNTs due to

the inter-tube interactions and negligible contribution of inter-tube phonon modes to the thermal conductivity of bundles [149, 150]. It also suggests that three-phonon umklapp scattering involving phonons from neighboring CNTs does not play any significant role in perfect bundles consisting of defect-free CNTs. The experimental observations of the pronounced decrease of the thermal conductivity of bundles with increasing bundle thickness [31, 145, 152], therefore, is likely to have alternative explanations, such as the higher degree of CNT misalignment and increased concentration of inter-tube defects, cross-links, and foreign inclusions in larger bundles, which could result in the increase of both the phonon scattering and inter-tube contact thermal resistance.

The second effect related to the inter-tube interactions, which has been a subject of contradictory computational predictions, is the influence of the contact density on the conductance of an individual contact. The results of atomistic Green's function calculations performed for both single and double contact junctions between (10,10) CNTs (configurations shown in Fig. 5.4d, e) have predicted an order of magnitude reduction of the contact conductance in a double junction with respect to an isolated junction [21]. This dramatic reduction of inter-tube conductance in the presence of neighboring junctions, if true, has major implications for interpretation of the experimental data for high-density CNT materials. The results of recent NEMD simulations performed for single and double junctions between 100 nm long (10,10) CNTs [81], however, predict very weak sensitivity to the presence of neighboring junctions even at the smallest distances that can be realized in real materials. The dependence of the inter-tube conductance per junction on the junction separation distance plotted in Fig. 5.8b indicates that the conductance across CNT-CNT junctions is unaffected by the presence of neighboring junctions when the CNTs creating the junctions are outside the range of direct van der Waals interaction with each other. When junctions are created by CNTs separated by the minimum distance (equilibrium distance between CNTs), the conductance per junction is reduced by only $\sim 10\%$ with respect to an isolated CNT-CNT contact. While these results are in a sharp contrast with predictions of [21] discussed above, they are closer to the results of NEMD simulations reported in [80], where a somewhat stronger $\sim 20\%$ reduction in conductance per junction is observed for double junctions made up of 60 nm long (6,6) CNTs separated by relatively large distances of 10 or 20 nm, but no significant reduction in conductance is observed for neighboring junctions between 30 and 90 nm long nanotubes separated by 10 nm.

5.4 Mesoscopic Modeling of Thermal Transport in CNT Network Materials

The results of the atomistic simulations briefly reviewed above have provided a wealth of information on the intrinsic thermal conductivity of individual CNTs, its dependence on defects and elastic deformation, as well as the inter-tube contact

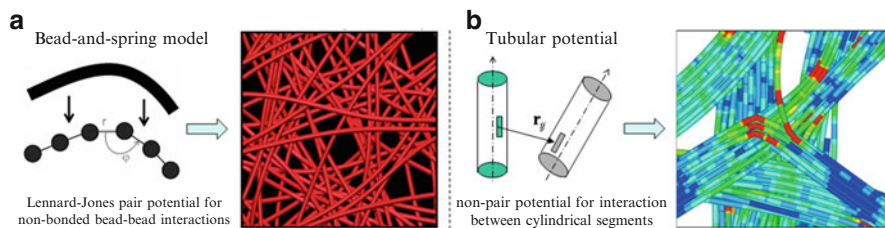


Fig. 5.9 Schematic representation of two descriptions of van der Waals inter-tube interactions adopted in the bead-and-spring model [83] (a) and in the mesoscopic model with tubular potential developed in [82, 84] (b). The *right panels* in (a, b) show fragments of CNT networks obtained with the two models, as reported in [85] and [87], respectively. In (b), the CNTs are colored by local radii of curvature, with red marking the segments adjacent to buckling kinks. Large artificial barriers inherent for the bead-and-spring model impede relative sliding of CNTs and prohibit formation of a network of bundles. In contrast, a network of bundles forms naturally in the dynamic simulation performed with the tubular potential

conductance for various contact configurations. The translation of all this information to the effective (macroscopic) thermal conductance of CNT materials, however, is far from being straightforward and requires a clear understanding of the collective heat transfer through thousands of nanotubes arranged into complex interconnected network structures. The gap between the predictions of atomistic simulations and the effective thermal transport properties of CNT materials can be bridged with the help of emerging mesoscopic computational models [82–101] capable of describing the collective behavior and properties of large groups of interacting nanotubes while still retaining the critical information on the individual nanotubes and their interactions revealed in the atomistic simulations. In this section, a brief overview of the mesoscopic models and their ability to reproduce structural self-organization of CNTs into continuous networks of bundles characteristic of real CNT materials is provided first, and is followed by a discussion of the mesoscopic calculations of thermal transport properties of the CNT network materials.

The mesoscopic models of CNT materials adopt coarse-grained representations of nanotubes, with the dynamic degrees of freedom of the models describing the motion of the nanotube segments composed of many atoms [82–84, 95]. Several alternative mesoscopic models proposed for CNT materials have similar formulations of the internal parts of the mesoscopic force fields that account for stretching, bending, and torsional deformation of individual nanotubes and are parameterized based on the results of atomistic simulations [82, 83, 86, 87, 90, 93, 95]. The different models, however, can be clearly distinguished by the computational approaches used for the description of the non-bonded van der Waals inter-tube interactions.

The most straightforward approach to the description of CNT–CNT interactions is suggested in [83] and is based on the bead-and-spring model commonly used in simulations of polymers [147]. In this model, the van der Waals inter-tube interactions are represented through the spherically symmetric pair-wise interactions

between mesoscopic segments of the nanotubes (Fig. 5.9a). Due to the simplicity of this approach, it has been adopted by several groups for analysis of the structure and mechanical properties of CNT materials [89, 91–93, 96, 98, 99]. An important drawback of this approach, however, is the existence of large artificial barriers for relative displacements of neighboring CNTs introduced by the pair-wise interactions between the “beads” in the bead-and-spring model [87, 95]. The presence of these barriers casts doubt on the ability of the model to provide an adequate description of the mechanical properties of the CNT materials and may prevent long-range rearrangements of CNTs required for their self-assembly into continuous networks of bundles. The latter effect can be illustrated by a snapshot from a simulation of a layer-by-layer deposition of straight randomly oriented CNTs shown in Fig. 5.9a. The bead-and-spring model predicts interlocking of the deposited nanotubes into a stable layered structure of randomly oriented individual CNTs [85, 98] which, experimentally, can only be stabilized by chemical functionalization or charging of the CNTs [148].

More advanced descriptions of non-bonding inter-tube interactions that do not result in the artificial corrugated inter-tube interactions have been developed and include the distinct element method [94, 95, 97] and the mesoscopic model adopting the tubular potential method for evaluation of the inter-tube interactions [82, 84]. As shown in Figs. 5.9b and 5.10a, b, the same procedure of layer-by-layer deposition of straight randomly oriented CNTs simulated with the tubular potential method results in a spontaneous self-assembly of CNTs into a continuous network of bundles with partial hexagonal ordering of CNTs in the bundles (Fig. 5.10b) and structural characteristics similar to the ones observed experimentally, e.g., [1–11]. The structure of the simulated CNT networks can be to a large extent controlled by parameters of the computational procedures used for the generation of the computational samples, and can be fine-tuned to match the results of experimental characterization. In particular, two distinct CNT structures, a CNT film and a “forest” of vertically aligned carbon nanotubes (VACNT), produced in mesoscopic simulations are shown in Fig. 5.10a, c along with experimental images of corresponding structures.

The availability of the computational samples reproducing the mesoscopic structure of real CNT materials opens up a broad range of opportunities for investigation of the dependence of the thermal transport properties on various material characteristics (material density, CNT type and length, density of cross-links, pore and bundle size distributions, degree of anisotropy in CNT orientation, etc.). First mesoscopic calculations of thermal conductivity performed for CNT films with preferential in-plane nanotube orientation [60, 100, 101], VACNT forests, and close-packed bundles of CNTs [79] have already provided important insights into the mechanisms and channels of the heat transfer in CNT network materials and are briefly discussed below.

Contrary to the conventional atomic-level MD simulations, the values of thermal conductivity of mesoscopic samples cannot be directly obtained from the analysis of the dynamic behavior of the coarse-grained elements of the model, and the calculation has to rely on special rules governing the heat transfer within and

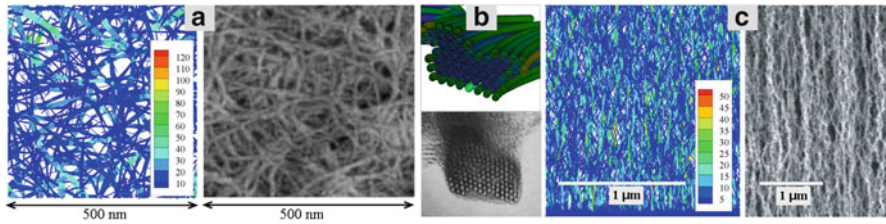


Fig. 5.10 Structure of CNT networks generated in mesoscopic simulations and observed experimentally. The experimental images of (a) buckypaper, (b) cross-section of a bundle, and (c) VACNT forest (all composed of single-walled CNTs) are from [8], [17], and [153], respectively. The computational images are for a CNT film consisting of 8000 200-nm-long (10,10) CNTs in (a) and a VACNT forest composed of 20,438 2- μm -long CNTs in (c). An enlarged view of a cross-section of a typical bundle is shown in (b). The computational samples have densities of 0.2 g/cm^3 in (a) and 0.02 g/cm^3 in (c), and dimensions of $0.5 \times 0.5 \times 0.1 \mu\text{m}^3$ in (a) and $2 \times 2 \times 2 \mu\text{m}^3$ in (c). Only a 20-nm-thick slice of the sample is shown in (a)

between the individual nanotubes. The complex structure of the entangled CNT networks introduces ambiguity in the concept of CNT–CNT contact area and calls for the design of a “heat transfer” function that accounts for the broad range of possible geometrical arrangements of the interacting CNT segments. As discussed above, in Sect. 5.3, a general description of the inter-tube conductance can be designed based on the results of atomistic simulations performed for various types of CNT–CNT contact configurations (see Fig. 5.7). The first mesoscopic simulations, however, were performed before the complete picture of the angular dependence of the contact conductance had emerged from the atomistic simulations and a simplified version of the heat transfer function [60, 79, 100, 101] that still ensured a continuous transition between the limiting cases of the inter-tube conductance between parallel and perpendicular CNTs was adopted in these simulations. Once the assumptions on the intrinsic thermal conductivity of individual CNTs and the CNT–CNT thermal conductance are made, the values of thermal conductivity of CNT networks generated in the dynamic mesoscopic simulations can be calculated by a method that is schematically illustrated in Fig. 5.11a. The opposing sides of a sample generated in a mesoscopic simulation are connected to the hot and cold heat reservoirs, the temperatures of all CNT segments located within the heat reservoirs are fixed at T_1 and T_2 , the temperatures of all “internal” CNTs are iteratively calculated from the balance of incoming and outgoing heat fluxes in each CNT or, in general, based on the solution of a system of one-dimensional heat conduction equations describing the heat propagation along nanotubes and energy exchange between them. Once the steady-state distribution of temperature is obtained, the heat flux Q through the sample can be determined, and the value of the effective thermal conductivity k of the CNT sample can be calculated from the Fourier law.

The results of the mesoscopic calculations of in-plane and out-of-plane conductivities of CNT films with preferential in-plane orientation of nanotubes arranged into continuous networks of bundles are shown in Fig. 5.11b. A striking result

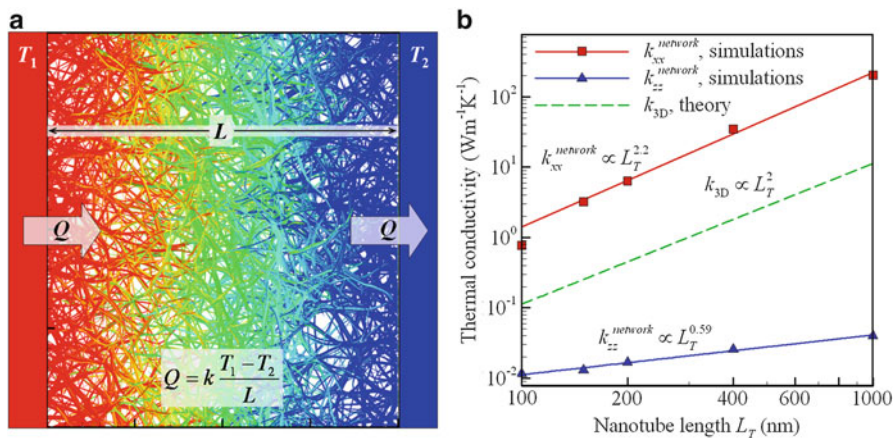


Fig. 5.11 Schematic of the method used in the calculation of thermal conductivity of CNT materials (a) and the values of the thermal conductivity predicted in simulations performed for systems composed of (10,10) CNTs of various length L_T and fixed material density of 0.2 g cm^{-3} [100]. The nanotubes in (a) are colored by their temperature and only a slice of the material with thicknesses of 50 nm is shown. The symbols in (b) show the results of the mesoscopic calculations, with red squares and blue triangles corresponding to the in-plane and out-of-plane conductivities of the anisotropic networks. The dashed line in (b) shows the prediction of an analytical scaling law obtained for a random distribution of straight CNTs (Eq. (5.1)) and discussed below, in Sect. 5.5

of these calculations is the large difference (more than two orders of magnitude) between the values of thermal conductivity predicted for the two directions in the material. The thermal conductivity within the plane of preferred orientation of CNTs, $k_{xx}^{network}$, increases from 0.8 to $205 \text{ Wm}^{-1} \text{ K}^{-1}$ as the length of CNTs increases from 100 nm to $1 \mu\text{m}$, whereas the conductivity perpendicular to the plane, $k_{zz}^{network}$, increases from 0.01 to $0.04 \text{ Wm}^{-1} \text{ K}^{-1}$ within the same range of nanotube lengths. The strong structural dependence of the thermal conductivity predicted in the simulations provides a clue for explaining the large variability of experimental data on thermal conductivity reported in literature, with values measured for various CNT materials ranging from ~ 0.02 to $\sim 1000 \text{ Wm}^{-1} \text{ K}^{-1}$ [14, 15, 21–34]. At the same time, the anisotropy of heat conduction and different scaling of the in-plane and out-of-plane conductivities with the CNT length, $k_{xx}^{network} \propto L_T^{2.2}$ and $k_{zz}^{network} \propto L_T^{0.59}$, support the feasibility of designing CNT-based materials capable of controlling and directing the heat flow along a desired path in thermal management applications.

The mesoscopic simulations discussed above and illustrated in Fig. 5.11 are done under assumption of a negligible contribution of the intrinsic thermal resistance of CNTs to the effective thermal resistance of a CNT material, which is thought to be largely defined by the inter-tube contact resistance. This assumption, commonly made in theoretical studies of heat transfer in CNT materials, e.g., [21, 72, 100], was critically evaluated in recent mesoscopic simulations that accounted for the finite intrinsic thermal conductivity of CNTs [101]. The results of the simulations,

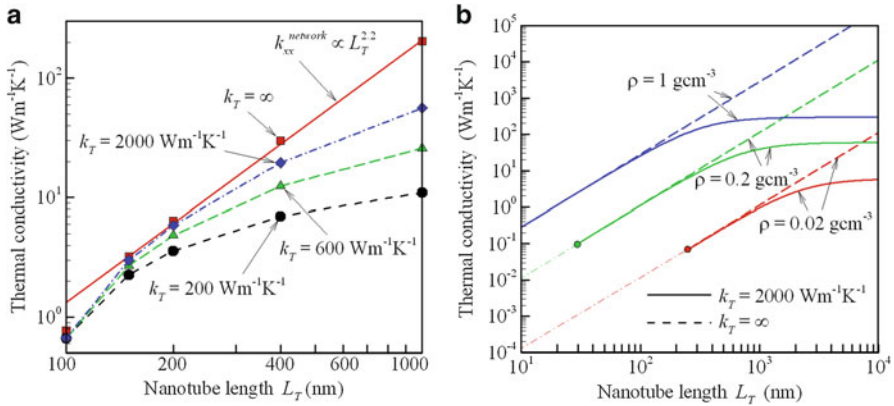


Fig. 5.12 Thermal conductivity of continuous networks of CNT bundles generated in mesoscopic simulations (a) and samples composed of straight randomly distributed CNTs (b) predicted for different values of intrinsic CNT conductivity k_T , nanotube length L_T , and material density ρ [101]. The material density of all networks in (a) is 0.2 g cm^{-3} . The solid and dashed lines in (b) show the predictions of Eq. (5.2) for $k_T = 2000 \text{ Wm}^{-1} \text{K}^{-1}$ and $k_T = \infty$, respectively, and a constant value of inter-tube conductance of $\sigma_c = 5 \times 10^{-11} \text{ WK}^{-1}$. The red and green circles mark the validity limit of the quadratic scaling of the conductivity with L_T as the system is approaching the percolation threshold

illustrated in Fig. 5.12a, have revealed an unexpectedly strong contribution of the intrinsic thermal resistance of CNTs that is found to make the dominant contribution to the effective thermal resistance of materials composed of CNTs that are longer than several hundreds of nanometers. Even for a relatively high intrinsic conductivity $k_T = 2000 \text{ Wm}^{-1} \text{K}^{-1}$ (see Table 5.1) and $L_T = 1 \mu\text{m}$, the value of the effective conductivity of the CNT network is ~ 3.5 times smaller than that predicted under assumption of negligible contribution of the intrinsic thermal resistance of CNTs, i.e., $k_T = \infty$. Further increase of the length of the nanotubes with finite values of k_T results in the saturation of the thermal conductivity of the materials at a level that is defined by the volume fraction of nanotubes (or density of the material). The physical origin of the strong effect of the intrinsic thermal resistance of the CNTs is explained by a theoretical analysis that provides scaling laws for thermal conductivity of samples composed of randomly dispersed straight CNTs [101]. The results of this analysis are illustrated in Fig. 5.12b and discussed in Sect. 5.5.

The effect of the intrinsic thermal resistance of the CNTs on the effective conductivity of CNT network materials can be amplified by the contributions from various structural defects and elastic deformation of CNTs. As discussed in Sect. 5.2 and illustrated in Fig. 5.3, the results of atomistic simulations reveal a substantial increase of the thermal resistance of nanotubes undergoing mechanical deformation and buckling. Mesoscopic modeling provides opportunities to translate the predictions of the atomistic simulations to the effective conductivity of CNT-based materials. In particular, the implications of the finite thermal conductance of the buckling kinks on the conductivity of CNT-based materials have been

investigated in mesoscopic calculations performed for films composed of thousands of CNTs arranged into continuous networks of bundles [60]. The mesoscopic calculations predict a substantial contribution of the angular-dependent thermal resistance of the buckling kinks to the thermal conductivity of CNT-based materials, which is amplified by the preferential buckling of thin bundles and individual CNTs serving as interconnections between thicker bundles in the network structures. The total heat flux passing through the CNTs that are parts of the interconnections is, on average, higher than in other parts of the network structures. Consequently, the high concentration of the buckling kinks in interconnects results in a stronger impact of the buckling on the overall thermal conductivity of the films.

A recent series of calculations performed for VACNT “forests” consisting of 2 μm long (10,10) CNTs also predict a noticeable, up to 15 %, reduction of the thermal conductivity in the direction of the preferential orientation of nanotubes when the thermal resistance of the buckling kinks is accounted for in the calculations. The corresponding change in the heat flux along the nanotubes is illustrated in Fig. 5.13 for one of the simulated VACNT samples. Note that the sample used in these calculations is fully relaxed and all buckling kinks appear as a result of spontaneous self-organization of individual CNTs into bundles. The number of the buckling kinks can be expected to increase dramatically in the course of mechanical deformation, when the collective buckling is known to occur in response to compressive loading, e.g., [151, 154]. While the onset of collective buckling is likely to lead to a substantial drop in the effective thermal conductivity of the CNT material, the extent of this drop is defined by complex redistribution of the heat flux in response to the appearance of new “thermal resistors” and cannot be evaluated simply based on the average density of the buckling kinks. The mesoscopic modeling of heat transfer provides a unique opportunity for investigation of the changing pathways of the heat flow in CNT materials undergoing mechanical deformation.

5.5 Derivation of Scaling Laws and Monte Carlo Simulations

The results of the mesoscopic simulations discussed above can be related to theoretical models for thermal and electrical conductivity of nanofibrous materials [72, 100–114]. While different in details, these models are based on assumptions of straight dispersed nanotubes with point inter-tube contacts responsible for the heat exchange between CNTs. As a result, these models are not capable of quantitative description of the heat transport in continuous networks of CNTs, where the nanotubes are arranged into bundles and the interconnections between bundles are playing a prominent role. Nevertheless, the theoretical analysis performed with simplified models can be used for revealing the basic scaling laws with respect to key material parameters and can provide general guidance for designing CNT materials with improved thermal transport properties.

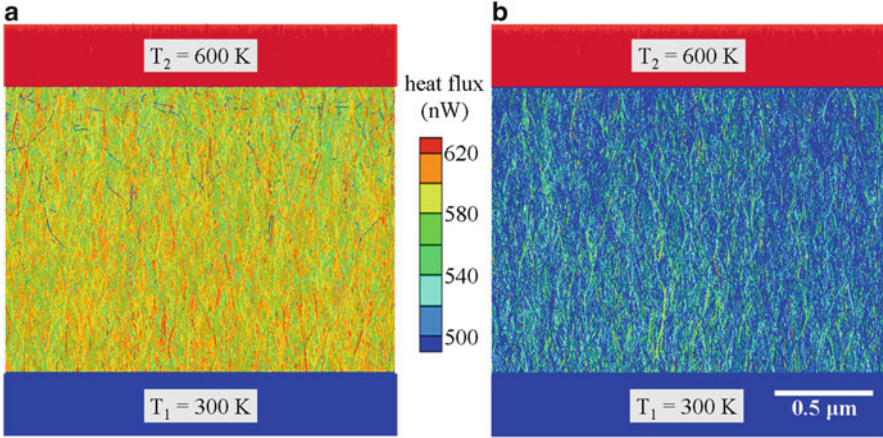


Fig. 5.13 The steady-state heat flux along the nanotubes obtained in the calculations of thermal conductivity of a VACNT sample consisting of 20,438 2- μm -long (10,10) CNTs. The same intrinsic thermal conductivity of $2000 \text{ Wm}^{-1} \text{ K}^{-1}$ is assumed for buckling-free CNTs in both calculations. The thermal resistance of buckling kinks is neglected in the calculation illustrated in (a) and is accounted for in (b). The values of the effective thermal conductivity of the VACNT sample predicted in the two calculations are 16.4 and $13.9 \text{ Wm}^{-1} \text{ K}^{-1}$, respectively

The capabilities and limitations of the theoretical approach to the analysis of the heat transfer in CNT network materials can be illustrated by the results of a recent study where a three-dimensional (3D) system composed of straight randomly dispersed nanotubes of length L_T and radius R_T is considered [100]. In this work, the derivation of the effective thermal conductivity of the CNT network is based on the ensemble averaging over configurational space performed under assumption of homogeneous and isotropic distribution of individual nanotubes in a system where a fixed temperature gradient is established. With an additional assumption of the dominant contribution of the inter-tube thermal contact resistance to the effective thermal resistance of the material (i.e., the intrinsic thermal resistance of CNTs is neglected and individual CNTs are considered to be isothermal), the following theoretical equation can be obtained:

$$k_{3D} = \frac{\sigma_c}{R_T} \frac{\pi \bar{n}_V^2}{36} \left(1 + 16\bar{R}_T + 80\bar{R}_T^2 + 192\bar{R}_T^3 + 153.6\bar{R}_T^4 \right), \quad (5.1)$$

where $\bar{n}_V = n_V L_T^2 R_T$ is the dimensionless density parameter, n_V is the volume number density of CNTs in the sample, \bar{R}_T is the ratio of CNT radius R_T to its length L_T , $\bar{R}_T = R_T/L_T$, and σ_c is the inter-tube contact conductance (different from σ_T used in the discussion of inter-tube conductance per unit length for parallel CNTs in Sect. 5.3).

Since the material mass density, ρ , is proportional to $n_V L_T$, Eq. (5.1) predicts a quadratic dependence of the thermal conductivity on both ρ and L_T , $k_{3D} \propto \rho^2 L_T^2$.

This scaling law is in agreement with the results of Monte Carlo simulations of the electrical conductivity of 3D percolating networks dominated by contact resistance [102], where the quadratic scaling with density was observed. The scaling law $k_{3D} \propto \rho^2 L_T^2$ is also consistent with the results of a theoretical analysis of 3D systems of high aspect ratio rod-like particles [107, 108], which reveals the quadratic dependence on both rod length and density in the limit of dense systems. Recently, the quadratic scaling of thermal conductivity of the CNT films with material density was confirmed experimentally [113].

It is instructive to compare the predictions of the scaling law derived for randomly arranged straight CNTs and given by Eq. (5.1) with the results of the mesoscopic simulations performed for continuous networks of intertwined CNT bundles and discussed in Sect. 5.4. The results obtained for systems of (10,10) CNTs with the same material density of 0.2 g cm^{-3} and the value of contact conductance between the nanotubes crossing each other at a 90° angle, $\sigma_c = 5 \times 10^{-11} \text{ WK}^{-1}$, used in Eq. (5.1) are shown in Fig. 5.11b. Although the quadratic dependence on L_T predicted by Eq. (5.1) is similar to the super-quadratic dependence $k_{xx}^{network} \propto L_T^{2.2}$ observed for the random networks of CNT bundles produced in the mesoscopic simulations, the values of thermal conductivity in the networks of bundles significantly, by more than an order of magnitude, exceed the values predicted for the random arrangements of individual nanotubes. This difference can be attributed to the bundle structure of the CNT networks [100]. The tight arrangements of CNTs in the bundles result in a larger CNT–CNT contact area as compared to the random arrangements of CNTs assumed in the derivations of Eq. (5.1). Thus, we can conclude that while the model of straight individual nanotubes is commonly used in interpretation of the results of experimental measurements, the thermal conductivity of real nanotube materials is likely to be strongly enhanced by self-organization of CNTs into continuous networks of bundles. The design of the analytical description (scaling laws) capable of accounting for the realistic structure of real CNT materials is an outstanding challenge on the way of providing an adequate quantitative description of the thermal transport properties of CNT materials.

The validity of the assumption of negligible effect of the intrinsic thermal resistance of CNTs on the effective conductivity of CNT network materials is evaluated in a recent study [101] where the simplification of isothermal nanotubes is relaxed and the temperature distributions along individual nanotubes are calculated by solving one-dimensional heat conduction equations along every CNTs and accounting for both the intrinsic thermal conductivity and the heat exchange with surrounding nanotubes. In this case, the evaluation of thermal conductivity within the theoretical framework similar to that used in [100] for isothermal nanotubes results in the following equation:

$$k'_{3D} = \frac{k_{3D}}{1 + \text{Bi}_c \langle N_J \rangle / 12} = \frac{k_{3D}}{1 + \text{Bi}_T / 12}, \quad (5.2)$$

where k_{3D} is the thermal conductivity of the CNT network at $k_T = \infty$, given by Eq. (5.1), $\text{Bi}_T = \text{Bi}_c \langle N_J \rangle = \sigma_c \langle N_J \rangle L_T / (k_T A_T)$ is a dimensionless parameter, $\langle N_J \rangle$ is the ensemble-averaged number of thermal contacts per CNT, and A_T is the cross-sectional area of a CNT. The parameter Bi_T is defined by the ratio of the total contact conductance $\sigma_c \langle N_J \rangle$ of a nanotube at all contacts it has with other CNTs to the intrinsic conductance of the nanotube, $k_T A_T / L_T$, and can be referred to as a Biot number for a nanotube. Similarly to the conventional definition of the Biot number in heat transfer analysis, the value of Bi_T can be used as a measure of non-isothermal distribution of temperature in an individual nanotube. The value of Bi_T , which increases with increasing material density and L_T , can be fairly large for real materials even if the ratio of the conductance in a single contact to the intrinsic conductance of the CNT, $\sigma_c L_T / (k_T A_T)$, is small.

The predictions of Eq. (5.2) are illustrated in Fig. 5.12b, where the solid curves show the dependence of k'_{3D} on L_T , for 3D samples composed of randomly oriented and distributed (10,10) CNTs for three values of material density ρ , typical of the CNT films and buckypaper. At small L_T , k'_{3D} practically coincides with k_{3D} (dashed curves in Fig. 5.12b) and scales quadratically with both ρ and L_T . An increase of L_T at a fixed ρ also increases Bi_T and results in the deviation of k'_{3D} from k_{3D} as Bi_T approaches and exceeds unity. In the limit of infinitely large Bi_T , the conductivity approaches an asymptotic value that is independent of L_T and linearly proportional to ρ . Somewhat unexpectedly, the transition between the two limiting scaling laws, $k \propto \rho^2 L_T^2$ at $\text{Bi}_T = 0$ and $k \propto \rho$ at $\text{Bi}_T \rightarrow \infty$ is observed for relatively short CNTs, on the order of hundreds of nanometers. The theoretical predictions given in Eq. (5.2) are consistent with the results of mesoscopic simulations discussed in Sect. 5.4 and illustrated in Fig. 5.12a. Thus, contrary to the common assumption of the dominant effect of the contact conductance, we can conclude that the intrinsic CNT conductivity, rather than contact conductance, is defining the overall thermal conductivity of CNT materials composed of nanotubes with the characteristic length on the order of micrometers or longer.

5.6 Concluding Remarks

The complexity of structural organization of CNT network materials is presenting a challenge for predictive modeling of their thermal transport properties and calls for a tightly integrated multiscale computational approach to this challenging problem. The applications of well-established atomistic simulation techniques and emerging mesoscopic models to the investigation of various aspects the heat transport in CNT materials have already resulted in a substantial progress in the fundamental understanding of the mechanisms and pathways of the heat transfer in different types of CNT materials. The results of atomistic simulations, in particular, have clarified a number of questions related to the heat transfer in individual CNTs and CNT–CNT heat conduction. The length dependence of the intrinsic thermal conductivity of CNTs, the conditions defining the transition from ballistic to diffusive phonon

transport regimes, the effect of the structural defects and various modes of elastic and inelastic deformation on the conductivity of CNTs are among the questions that have been addressed in atomistic simulations of individual nanotubes and briefly reviewed in Sect. 5.2. The atomistic simulations of two or more interacting nanotubes have also been performed and provided important information on the inter-tube contact conductance, its dependence on the contact area, geometrical characteristics of the contact, as well as proximity of other contacts. A number of research questions related to the inter-tube conductance, including the ones that have been subjects of contradictory claims and controversial discussion in literature, are critically reviewed in Sect. 5.3. The results of mesoscopic modeling of the collective heat transfer by thousands of CNTs arranged into interconnected networks of bundles are reviewed in Sect. 5.4. While the development of mesoscopic models is still at the very early stage and many challenging technical issues still remain to be resolved, the first results of mesoscopic calculations are promising and demonstrate the ability of mesoscopic models to provide a bridge between the insights obtained in the atomistic simulations and the effective thermal conductance of CNT materials. Moreover, some of the predictions of the mesoscopic simulations, such as the strong (more than an order of magnitude) enhancement of the heat transfer in CNT materials due to the self-organization of CNTs into continuous networks of bundles or the dominant contribution of the intrinsic thermal resistance of CNTs to the effective thermal resistance of CNT materials composed of nanotubes that are longer than several hundreds of nanometers, are rather unexpected and make a strong impact on interpretation of experimental observations.

An apparent conclusion emerging from the overview of the computational results presented in this chapter is the one on the critical importance of combining the results obtained by different methods and dealing with processes occurring at different time and length scales into a well-integrated multiscale physical model of the heat transfer in CNT materials. In particular, the results of atomistic simulations can be used to design a reliable description of the inter-tube conductance suitable for incorporation into mesoscopic models which, in turn, can yield the information on the structural dependence of the thermal transport properties and stimulate the development of advanced theoretical models. Further insights obtained in atomistic studies of the effects of cross-links, polymer wrapping, or metal coating on the intrinsic conductivity of CNTs and the inter-tube conductance can be incorporated into the mesoscopic models and used for the exploration of the space of the material design parameters and optimization of the thermal transport properties of CNT network materials. Moreover, the dynamic nature of the mesoscopic models opens up opportunities for investigation of the effect of mechanical deformation on thermal conductivity of CNT materials. Mesoscopic simulations can be used for evaluation of the changing pathways of the heat flow in materials undergoing mechanical deformation as well as the thermal transport signatures of critical events, such as the onset of coordinated buckling and local failure, leading to an improved understanding of the performance of CNT-based thermal interface materials under conditions when large deformations are introduced by the requirements of compliance with complex geometrical shapes of heat sinks and sources in microelectronic devices.

On the side of the theoretical analysis of the general structure—thermal transport properties relationships, one critical challenge is to go beyond the assumption of randomly dispersed straight nanotubes and to design analytical descriptions capable of connecting the structural characteristics of real CNT materials (material density, CNT type and length, density of cross-links, pore and bundle size distributions) to the thermal transport properties. The ability of the mesoscopic simulations to reproduce realistic structures of various CNT materials (aerogels, films, forests, and fibers) is likely to play an important role in the design and verification of the advanced theoretical models.

Acknowledgments The authors acknowledge financial support provided by the National Aeronautics and Space Administration (NASA) through an Early Stage Innovations grant from NASA's Space Technology Research Grants Program (NNX16AD99G) and by the Air Force Office of Scientific Research (AFOSR) through the AFOSR's Thermal Sciences program (FA9550-10-10545). Computational support is provided by the National Science Foundation (NSF) through the Extreme Science and Engineering Discovery Environment (Projects TG-DMR110090 and TG-DMR130010).

References

1. Zou J, Liu J, Karakoti AS, Kumar A, Joung D, Li Q, Khondaker SI, Seal S, Zhai L (2010) Ultralight multiwalled carbon nanotube aerogel. *ACS Nano* 4:7293–7302
2. Gui X, Cao A, Wei J, Li H, Jia Y, Li Z, Fan L, Wang K, Zhu H, Dehai C (2010) Soft, highly conductive nanotube sponges and composites with controlled compressibility. *ACS Nano* 4:2320–2326
3. Sreekumar TV, Liu T, Kumar S, Ericson LM, Hauge RH, Smalley RE (2003) Single-wall carbon nanotube films. *Chem Mater* 15:175–178
4. Hennrich F, Lebedkin S, Malik S, Tracy J, Barczewski M, Rösner H, Kappes M (2002) Preparation, characterization and applications of free-standing single walled carbon nanotube thin films. *Phys Chem Chem Phys* 4:2273–2277
5. Muramatsu H, Hayashi T, Kim YA, Shimamoto D, Kim YJ, Tantrakarn K, Endo M, Terrones M, Dresselhaus MS (2005) Pore structure and oxidation stability of double-walled carbon nanotube-derived buckypaper. *Chem Phys Lett* 414:444–448
6. Ma W, Song L, Yang R, Zhang T, Zhao Y, Sun L, Ren Y, Liu D, Liu L, Shen J, Zhang Z, Xiang Y, Zhou W, Xie S (2007) Directly synthesized strong, highly conducting, transparent single-walled carbon nanotube films. *Nano Lett* 7:2307–2311
7. Xu M, Futaba DN, Yumura M, Hata K (2012) Alignment control of carbon nanotube forest from random to nearly perfectly aligned by utilizing the crowding effect. *ASC Nano* 6: 5837–5844
8. Futaba DN, Hata K, Yamada T, Hiraoka T, Hayamizu Y, Kakudate Y, Tanaie O, Hatori H, Yumura M, Iijima S (2006) Shape-engineerable and highly densely packed single-walled carbon nanotubes and their application as super-capacitor electrodes. *Nat Mater* 5:987–994
9. Wang Z, Liang Z, Wang B, Zhang C, Kramer L (2004) Processing and property investigation of single-walled carbon nanotube (SWNT) buckypaper/epoxy resin matrix nanocomposites. *Compos Part A Appl Sci Manuf* 35:1225–1232
10. Whitten PG, Spinks GM, Wallace GG (2007) Mechanical properties of carbon nanotube paper in ionic liquid and aqueous electrolytes. *Carbon* 43:1891–1896
11. Whitby RLD, Fukuda T, Maekawa T, James SL, Mikhalovsky SV (2008) Geometric control and tuneable pore size distribution of buckypaper and buckydisks. *Carbon* 46:949–956

12. Poulin P, Vigolo B, Launois P (2002) Films and fibers of oriented single wall nanotubes. *Carbon* 40:1741–1749
13. Zhang X, Jiang K, Feng C, Liu P, Zhang L, Kong J, Zhang T, Li Q, Fan S (2006) Spinning and processing continuous yarn from 4-inch wafer scale super-aligned carbon nanotube arrays. *Adv Mater* 18:1505–1510
14. Behabtu N, Young CC, Tsentelovich DE, Kleinerman O, Wang X, Ma AWK, Bengio A, ter Waarbek RF, de Jong JJ, Hoogerwerf RE, Fairchild SB, Ferguson JB, Maruyama B, Kono J, Talmon Y, Cohen Y, Otto MJ, Pasquali M (2013) Strong, light, multifunctional fibers of carbon nanotubes with ultrahigh conductivity. *Science* 339:182–186
15. Zhang L, Zhang G, Liu C, Fan S (2012) High-density carbon nanotube buckypapers with superior transport and mechanical properties. *Nano Lett* 12:4848–4852
16. Girifalco LA, Hodak M, Lee RS (2000) Carbon nanotubes, buckyballs, ropes, and a universal graphitic potential. *Phys Rev B* 62:13104–13110
17. Thess A, Lee R, Nikolaev P, Dai H, Petit P, Robert J, Xu C, Lee YH, Kim SG, Rinzler AG, Colbert DT, Scuseria GE, Tománek D, Fischer JE, Smalley RE (1996) Crystalline ropes of metallic carbon nanotubes. *Science* 273:483–487
18. Rinzler AG, Liu J, Dai H, Nikolaev P, Huffman CB, Rodríguez-Macías FJ, Boul PJ, Lu AH, Heymann D, Colbert DT, Lee RS, Fischer JE, Rao AM, Eklund PC, Smalley RE (1998) Large-scale purification of single-wall carbon nanotubes: process, product, and characterization. *Appl Phys A Mater Sci Process* 67:29–37
19. Dettlaff-Weglikowska U, Skákalová V, Graupner R, Jhang SH, Kim BH, Lee HJ, Ley L, Park YW, Berber S, Tománek D, Roth S (2005) Effect of SOCl₂ treatment on electrical and mechanical properties of single-wall carbon nanotube networks. *J Am Chem Soc* 127: 5125–5131
20. Eom K, Nam K, Jung H, Kim P, Strano MS, Han J-H, Kwon T (2013) Controllable viscoelastic behavior of vertically aligned carbon nanotube arrays. *Carbon* 65:305–314
21. Prasher RS, Hu XJ, Chalopin Y, Mingo N, Lofgreen K, Volz S, Cleri F, Keblinski P (2009) Turning carbon nanotubes from exceptional heat conductors into insulators. *Phys Rev Lett* 102:105901
22. Hone J, Whitney M, Piskoti C, Zettl A (1999) Thermal conductivity of single-walled carbon nanotubes. *Phys Rev B* 59:R2514–R2516
23. Hone J, Whitney M, Zettl A (1999) Thermal conductivity of single-walled carbon nanotubes. *Synth Met* 103:2498–2499
24. Hone J, Llaguno MC, Nemes NM, Johnson AT, Fischer JE, Walters DA, Casavant MJ, Schmidt J, Smalley RE (2000) Electrical and thermal transport properties of magnetically aligned single wall carbon nanotube films. *Appl Phys Lett* 77:666–668
25. Hone J, Llaguno MC, Biercuk MJ, Johnson AT, Batlogg B, Benes Z, Fischer JE (2002) Thermal properties of carbon nanotubes and nanotube-based materials. *Appl Phys A* 74: 339–343
26. Gonnet P, Liang SY, Choi ES, Kadambala RS, Zhang C, Brooks JS, Wang B, Kramer L (2006) Thermal conductivity of magnetically aligned carbon nanotube buckypapers and nanocomposites. *Curr Appl Phys* 6:119–122
27. Yang DJ, Zhang Q, Chen G, Yoon SF, Ahn J, Wang SG, Zhou Q, Wang Q, Li JQ (2002) Thermal conductivity of multiwalled carbon nanotubes. *Phys Rev B* 66:165440
28. Yang DJ, Wang SG, Zhang Q, Sellin PJ, Chen G (2004) Thermal and electrical transport in multi-walled carbon nanotubes. *Phys Lett A* 329:207–213
29. Duong HM, Nguyen ST (2011) Limiting mechanisms of thermal transport in carbon nanotube-based heterogeneous media. *Recent Pat Eng* 5:209–232
30. Ivanov I, Puretzyk A, Eres G, Wang H, Pan Z, Cui H, Jin R, Howe J, Geohagan DB (2006) Fast and highly anisotropic thermal transport through vertically aligned carbon nanotube arrays. *Appl Phys Lett* 89:223110
31. Aliev AE, Lima MH, Silverman EM, Baughman RH (2010) Thermal conductivity of multi-walled carbon nanotube sheets: radiation losses and quenching of phonon modes. *Nanotechnology* 21:035709

32. Zhang G, Liu C, Fan S (2013) Directly measuring of thermal pulse transfer in one-dimensional highly aligned carbon nanotubes. *Sci Rep* 3:2549
33. Marconnet AM, Panzer MA, Goodson KE (2013) Thermal conduction phenomena in carbon nanotubes and related nanostructured materials. *Rev Mod Phys* 85:1295–1326
34. Zhang KJ, Yadav A, Kim KH, Oh Y, Islam MF, Uher C, Pipe KP (2013) Thermal and electrical transport in ultralow density single-walled carbon nanotube networks. *Adv Mater* 25:2926–2931
35. Berber S, Kwon Y-K, Tomanek D (2000) Unusually high thermal conductivity of carbon nanotubes. *Phys Rev Lett* 84:4613–4616
36. Che J, Çağın T, Goddard WA III (2000) Thermal conductivity of carbon nanotubes. *Nanotechnology* 11:65–69
37. Osman MA, Srivastava D (2001) Temperature dependence of the thermal conductivity of single-wall carbon nanotubes. *Nanotechnology* 12:21–24
38. Maruyama S (2002) A molecular dynamics simulation of heat conduction in finite length SWNTs. *Phys B* 323:193–195
39. Maruyama S (2003) A molecular dynamics simulation of heat conduction of a finite length single-walled carbon nanotube. *Microscale Thermophys Eng* 7:41–50
40. Padgett CW, Brenner DW (2004) Influence of chemisorption on the thermal conductivity of single-wall carbon nanotubes. *Nano Lett* 4:1051–1053
41. Moreland JF, Freund JB, Chen G (2004) The disparate thermal conductivity of carbon nanotubes and diamond nanowires studied by atomistic simulation. *Microscale Thermophys Eng* 8:61–69
42. Grujicic M, Cao G, Gersten B (2004) Atomic-scale computations of the lattice contribution to thermal conductivity of single-walled carbon nanotubes. *Mater Sci Eng B* 107:204–216
43. Grujicic M, Cao G, Roy WN (2005) Computational analysis of the lattice contribution to thermal conductivity of single-walled carbon nanotubes. *J Mater Sci* 40:1943–1952
44. Zhang G, Li B (2005) Thermal conductivity of nanotubes revisited: effects of chirality, isotope impurity, tube length, and temperature. *J Chem Phys* 123:114714
45. Bi K, Chen Y, Yang J, Wang Y, Chen M (2006) Molecular dynamics simulation of thermal conductivity of single-wall carbon nanotubes. *Phys Lett A* 350:150–153
46. Lukes JR, Zhong H (2007) Thermal conductivity of individual single-wall carbon nanotubes. *J Heat Transf* 129:705–716
47. Pan R-Q, Xu Z-J, Zhu Z-Y (2007) Length dependence of thermal conductivity of single-walled carbon nanotubes. *Chin Phys Lett* 24:1321–1323
48. Shiomi J, Maruyama S (2008) Molecular dynamics of diffusive-ballistic heat conduction in single-walled carbon nanotubes. *Jpn J Appl Phys* 47:2005–2009
49. Alaghemandi M, Algaer E, Bohm MC, Muller-Plathe F (2009) The thermal conductivity and thermal rectification of carbon nanotubes studied using reverse non-equilibrium molecular dynamics simulations. *Nanotechnology* 20:115704
50. Wu MCH, Hsu J-Y (2009) Thermal conductivity of carbon nanotubes with quantum correction via heat capacity. *Nanotechnology* 20:145401
51. Xu Z, Buehler MJ (2009) Strain controlled thermomutability of single-walled carbon nanotubes. *Nanotechnology* 20:185701
52. Nishimura F, Takahashi T, Watanabe K, Yamamoto T (2009) Bending robustness of thermal conductance of carbon nanotubes: nonequilibrium molecular dynamics simulation. *Appl Phys Express* 2:035003
53. Ren C, Zhang W, Xu Z, Zhu Z, Huai P (2010) Thermal conductivity of single-walled carbon nanotubes under axial stress. *J Phys Chem C* 114:5786–5791
54. Thomas JA, Iutzi RM, McGaughey AJH (2010) Thermal conductivity and phonon transport in empty and water-filled carbon nanotubes. *Phys Rev B* 81:045413
55. Shelly RA, Toprak K, Bayazitoglu Y (2010) Nose–Hoover thermostat length effect on thermal conductivity of single wall carbon nanotubes. *Int J Heat Mass Transf* 53:5884–5887
56. Lin C, Wang H, Yang W (2010) The thermomutability of single-walled carbon nanotubes by constrained mechanical folding. *Nanotechnology* 21:365708

57. Pan R-Q (2011) Diameter and temperature dependence of thermal conductivity of single-walled carbon nanotubes. *Chin Phys Lett* 28:066104
58. Wei N, Xu L, Wang H-Q, Zheng J-C (2011) Strain engineering of thermal conductivity in graphene sheets and nanoribbons: a demonstration of magic flexibility. *Nanotechnology* 22:105705
59. Qiu B, Wang Y, Zhao Q, Ruan X (2012) The effects of diameter and chirality on the thermal transport in free-standing and supported carbon-nanotubes. *Appl Phys Lett* 100:233105
60. Volkov AN, Shiga T, Nicholson D, Shiomi J, Zhigilei LV (2012) Effect of bending buckling of carbon nanotubes on thermal conductivity of carbon nanotube materials. *J Appl Phys* 111:053501
61. Nishimura F, Shiga T, Maruyama S, Watanabe K, Shiomi J (2012) Thermal conductance of buckled carbon nanotubes. *Jpn J Appl Phys* 51:015102
62. Cao A, Qu J (2012) Size dependent thermal conductivity of single-walled carbon nanotubes. *J Appl Phys* 112:013503
63. Imtani AN (2013) Thermal conductivity for single-walled carbon nanotubes from Einstein relation in molecular dynamics. *J Phys Chem Solids* 74:1599–1603
64. Feng D-L, Feng Y-H, Chen Y, Li W, Zhang X-X (2013) Effects of doping, Stone-Wales and vacancy defects on thermal conductivity of single-wall carbon nanotubes. *Chin Phys B* 22:016501
65. Zhu L, Li B (2014) Low thermal conductivity in ultrathin carbon nanotube (2,1). *Sci Rep* 4:4917
66. Salaway RN, Zhigilei LV (2014) Molecular dynamics simulations of thermal conductivity of carbon nanotube: resolving the effects of computational parameters. *Int J Heat Mass Transf* 70:954–964
67. Ma J, Ni Y, Volz S, Dumitrică T (2015) Thermal transport in single-walled carbon nanotubes under pure bending. *Phys Rev Appl* 3:024014
68. Säskilähti K, Oksanen J, Volz S, Tulkki J (2015) Frequency-dependent phonon mean free path in carbon nanotubes from nonequilibrium molecular dynamics. *Phys Rev B* 91:115426
69. Mehri A, Jamaati M, Moradi M (2015) The effect of imposed temperature difference on thermal conductivity in armchair single-walled carbon nanotube. *Int J Mod Phys C* 26:1550105
70. Zhong H, Lukes J (2006) Interfacial thermal resistance between carbon nanotubes: molecular dynamics simulations and analytical thermal modeling. *Phys Rev B* 74:125403
71. Maruyama S, Igarashi Y, Taniguchi Y, Shiomi J (2006) Anisotropic heat transfer of single-walled carbon nanotubes. *J Therm Sci Technol* 1:138–148
72. Chalopin Y, Volz S, Mingo N (2009) Upper bound to the thermal conductivity of carbon nanotube pellets. *J Appl Phys* 105:084301
73. Kumar S, Murthy JY (2009) Interfacial thermal transport between nanotubes. *J Appl Phys* 106:084302
74. Xu Z, Buehler MJ (2009) Nanoengineering heat transfer performance at carbon nanotube interfaces. *ACS Nano* 3:2767–2775
75. Varshney V, Patnaik SS, Roy AK, Farmer BL (2010) Modeling of thermal conductance at transverse CNT-CNT interfaces. *J Phys Chem C* 114:16223–16228
76. Evans WJ, Koblinski P (2010) Thermal conductivity of carbon nanotube cross-bar structures. *Nanotechnology* 21:475704
77. Evans WJ, Shen M, Koblinski P (2012) Inter-tube thermal conductance in carbon nanotubes arrays and bundles: effects of contact area and pressure. *Appl Phys Lett* 100:261908
78. Hu G-J, Cao B-Y (2013) Thermal resistance between crossed carbon nanotubes: molecular dynamics simulations and analytical modeling. *J Appl Phys* 114:224308
79. Volkov AN, Salaway RN, Zhigilei LV (2013) Atomistic simulations, mesoscopic modeling, and theoretical analysis of thermal conductivity of bundles composed of carbon nanotubes. *J Appl Phys* 114:104301
80. Hu L, McGaughey AJH (2014) Thermal conductance of the junction between single-walled carbon nanotubes. *Appl Phys Lett* 105:193104

81. Salaway RN, Zhigilei LV (2016) Thermal conductance of carbon nanotube contacts: molecular dynamics simulations and general description of the contact conductance. Submitted
82. Zhigilei LV, Wei C, Srivastava D (2005) Mesoscopic model for dynamic simulations of carbon nanotubes. *Phys Rev B* 71:165417
83. Buehler M (2006) Mesoscale modeling of mechanics of carbon nanotubes: self-assembly, self-folding, and fracture. *J Mater Res* 21:2855–2869
84. Volkov AN, Zhigilei LV (2010) Mesoscopic interaction potential for carbon nanotubes of arbitrary length and orientation. *J Phys Chem C* 114:5513–5531
85. Cranford SW, Buehler MJ (2010) *In silico* assembly and nanomechanical characterization of carbon nanotube buckypaper. *Nanotechnology* 21:265706
86. Anderson T, Akatyeva E, Nikiforov I, Potyondy D, Ballarini R, Dumitrică T (2010) Towards distinct element method simulations of carbon nanotube systems. *J Nanotechnol Eng Med* 1:041009
87. Volkov AN, Zhigilei LV (2010) Structural stability of carbon nanotube films: the role of bending buckling. *ACS Nano* 4:6187–6195
88. Zhigilei LV, Volkov AN, Leveugle E, Tabetah M (2011) The effect of the target structure and composition on the ejection and transport of polymer molecules and carbon nanotubes in matrix-assisted pulsed laser evaporation. *Appl Phys A* 105:529–546
89. Xie B, Liu Y, Ding Y, Zheng Q, Xu Z (2011) Mechanics of carbon nanotube networks: microstructural evolution and optimal design. *Soft Matter* 7:10039–10047
90. Jacobs WM, Nicholson DA, Zemer H, Volkov AN, Zhigilei LV (2012) Acoustic energy dissipation and thermalization in carbon nanotubes: atomistic modeling and mesoscopic description. *Phys Rev B* 86:165414
91. Wang C, Xie B, Liu Y, Xu Z (2012) Mechanotunable microstructures of carbon nanotube networks. *ACS Macro Lett* 1:1176–1179
92. Li Y, Kröger M (2012) Viscoelasticity of carbon nanotube buckypaper: zipping-unzipping mechanism and entanglement effects. *Soft Matter* 8:7822–7830
93. Li Y, Kröger M (2012) A theoretical evaluation of the effects of carbon nanotube entanglement and bundling on the structural and mechanical properties of buckypaper. *Carbon* 50:1793–1806
94. Wang Y, Gaidău C, Ostanin I, Dumitrică T (2013) Ring windings from single-wall carbon nanotubes: a distinct element method study. *Appl Phys Lett* 103:183902
95. Ostanin I, Ballarini R, Potyondy D, Dumitrică T (2013) A distinct element method for large scale simulations of carbon nanotube assemblies. *J Mech Phys Solids* 61:762–782
96. Won Y, Gao Y, Panzer MA, Xiang R, Maruyama S, Kenny TW, Cai W, Goodson KE (2013) Zipping, entanglement, and the elastic modulus of aligned single-walled carbon nanotube films. *Proc Natl Acad Sci USA* 110:20426–20430
97. Ostanin I, Ballarini R, Dumitrică T (2014) Distinct element method modeling of carbon nanotube bundles with intertube sliding and dissipation. *J Appl Mech* 81:061004
98. Zhao J, Jiang J-W, Wang L, Guo W, Rabczuk T (2014) Coarse-grained potentials of single-walled carbon nanotubes. *J Mech Phys Solids* 71:197–218
99. Maschmann MR (2015) Integrated simulation of active CNT forest growth and mechanical compression. *Carbon* 86:26–37
100. Volkov AN, Zhigilei LV (2010) Scaling laws and mesoscopic modeling of thermal conductivity in carbon nanotube materials. *Phys Rev Lett* 104:215902
101. Volkov AN, Zhigilei LV (2012) Heat conduction in carbon nanotube materials: strong effect of intrinsic thermal conductivity of carbon nanotubes. *Appl Phys Lett* 101:043113
102. Koblinski P, Cleri F (2004) Contact resistance in percolating networks. *Phys Rev B* 69:184201
103. Foygel M, Morris RD, Anez D, French S, Sobolev VL (2005) Theoretical and computational studies of carbon nanotube composites and suspensions: electrical and thermal conductivity. *Phys Rev B* 71:104201
104. Duong HM, Papavassiliou DV, Lee LL, Mullen KJ (2005) Random walks in nanotube composites: improved algorithms and the role of thermal boundary resistance. *Appl Phys Lett* 87:013101

105. Kumar S, Alam MA, Murthy JY (2007) Effect of percolation on thermal transport in nanotube composites. *Appl Phys Lett* 90:104105
106. Li J, Ma PC, Chow WS, To CK, Tang BZ, Kim J-K (2007) Correlations between percolation threshold, dispersion state, and aspect ratio of carbon nanotubes. *Adv Funct Mater* 17:3207–3215
107. Vassal J-P, Orgéas L, Favier D, Auriault J-L, Le Corre S (2008) Upscaling the diffusion equations in particulate media made of highly conductive particles. I. Theoretical aspects. *Phys Rev E* 77:011302
108. Vassal J-P, Orgéas L, Favier D, Auriault J-L, Le Corre S (2008) Upscaling the diffusion equations in particulate media made of highly conductive particles. II. Application to fibrous materials. *Phys Rev E* 77:011303
109. Duong HM, Papavassiliou DV, Mullen KJ, Maruyama S (2008) Computational modeling of the thermal conductivity of single-walled carbon nanotube–polymer composites. *Nanotechnology* 19:065702
110. Ashtekar NA, Jack DA (2009) Stochastic modeling of the bulk thermal conductivity for dense 1027 carbon nanotube networks. In: *Proceedings of ASME IMECE2009*, Paper IMECE2009-11282, Orlando, FL
111. Chalopin Y, Volz S, Mingo N (2010) Erratum: “Upper bound to the thermal conductivity of carbon nanotube pellets” [*J Appl Phys* 105:084301 (2009)]. *J Appl Phys* 108:039902
112. Bui KND, Grady BP, Papavassiliou DV (2011) Heat transfer in high volume fraction CNT nanocomposites: effects of inter-nanotube thermal resistance. *Chem Phys Lett* 508:248–251
113. Yamada Y, Nishiyama T, Yasuhara T, Takahashi K (2012) Thermal boundary conductance between multi-walled carbon nanotubes. *J Therm Sci Technol* 7:190–198
114. Žeželj M, Stanković I (2012) From percolating to dense random stick networks: conductivity model investigation. *Phys Rev E* 86:134202
115. Frenkel D, Smit B (1996) *Understanding molecular simulation: from algorithms to applications*. Academic, San Diego
116. Matsui M (1989) Molecular dynamics study of the structural and thermodynamic properties of MgO crystal with quantum correction. *J Chem Phys* 91:489–494
117. Levashov VA, Billinge SJL, Thorpe MF (2007) Quantum correction to the pair distribution function. *J Comput Chem* 28:1865–1882
118. Turney JE, McGaughey AJH, Amon CH (2009) Assessing the applicability of quantum corrections to classical thermal conductivity predictions. *Phys Rev B* 79:224305
119. Yonetani Y, Kinugawa K (2003) Transport properties of liquid para-hydrogen: the path integral centroid molecular dynamics approach. *J Chem Phys* 119:9651–9660
120. Wang J-S (2007) Quantum thermal transport from classical molecular dynamics. *Phys Rev Lett* 99:160601
121. Wang J-S, Ni X, Jiang J-W (2009) Molecular dynamics with quantum heat baths: application to nanoribbons and nanotubes. *Phys Rev B* 80:224302
122. Dammak H, Chalopin Y, Laroche M, Hayoun M, Greffet J-J (2009) Quantum thermal bath for molecular dynamics simulation. *Phys Rev Lett* 103:190601
123. Savin AV, Kosevich YA, Cantarero A (2012) Semiquantum molecular dynamics simulation of thermal properties and heat transport in low-dimensional nanostructures. *Phys Rev B* 86:064305
124. Bedoya-Martínez ON, Barrat J-L, Rodney D (2014) Computation of the thermal conductivity using methods based on classical and quantum molecular dynamics. *Phys Rev B* 89:014303
125. Hernández-Rojas J, Calvo F, Gonzalez Noya E (2015) Applicability of quantum thermal baths to complex many-body systems with various degrees of anharmonicity. *J Chem Theory Comput* 11:861–870
126. Evans DJ (1982) Homogeneous NEMD algorithm for thermal conductivity—application of non-canonical linear response theory. *Phys Lett A* 91:457–460
127. Tersoff J (1988) New empirical approach for the structure and energy of covalent systems. *Phys Rev B* 37:6991–7000
128. Tersoff J (1988) Empirical interatomic potential for carbon, with applications to amorphous carbon. *Phys Rev Lett* 61:2879–2882

129. Lindsay L, Broido DA (2010) Optimized Tersoff and Brenner empirical potential parameters for lattice dynamics and phonon thermal transport in carbon nanotubes and graphene. *Phys Rev B* 81:205441
130. Brenner DW (1990) Empirical potential for hydrocarbons for use in simulating the chemical vapor deposition of diamond films. *Phys Rev B* 42:9458–9471
131. Brenner DW, Shenderova OA, Harrison JA, Stuart SJ, Ni B, Sinnott SB (2002) A second-generation reactive empirical bond order (REBO) potential energy expression for hydrocarbons. *J Phys Condens Matter* 14:783–802
132. Stuart SJ, Tutein AB, Harrison JA (2000) A reactive potential for hydrocarbons with intermolecular interactions. *J Chem Phys* 112:6472–6486
133. Yu C, Shi L, Yao Z, Li D, Majumdar A (2005) Thermal conductance and thermopower of an individual single-wall carbon nanotube. *Nano Lett* 5:1842–1846
134. Pop E, Mann D, Wang Q, Goodson K, Dai H (2006) Thermal conductance of an individual single-wall carbon nanotube above room temperature. *Nano Lett* 6:96–100
135. Wang J, Wang J-S (2006) Carbon nanotube thermal transport: ballistic to diffusive. *Appl Phys Lett* 88:111909
136. Donadio D, Galli G (2007) Thermal conductivity of isolated and interacting carbon nanotubes: comparing results from molecular dynamics and the Boltzmann transport equation. *Phys Rev Lett* 99:255502
137. Mingo N, Broido DA (2005) Length dependence of carbon nanotube thermal conductivity and the “problem of long waves,”. *Nano Lett* 5:1221–1225
138. Mingo N, Broido DA (2005) Carbon nanotube ballistic thermal conductance and its limits. *Phys Rev Lett* 95:096105
139. Huxtable ST, Cahill DG, Shenogin S, Xue L, Ozisik R, Barone P, Usrey M, Strano MS, Siddons G, Shim M, Koblinski P (2003) Interfacial heat flow in carbon nanotube suspensions. *Nat Mater* 2:731–734
140. Yang J, Waltermire S, Chen Y, Zinn AA, Xu TT, Li D (2010) Contact thermal resistance between individual multiwall carbon nanotubes. *Appl Phys Lett* 96:023109
141. Yang J, Shen M, Yang Y, Evans WJ, Wei Z, Chen W, Zinn AA, Chen Y, Prasher R, Xu TT, Koblinski P, Li D (2014) Phonon transport through point contacts between graphitic nanomaterials. *Phys Rev Lett* 112:205901
142. Hsu I-K, Pettes MT, Aykol M, Chang C-C, Hung W-H, Theiss J, Shi L, Cronin SB (2011) Direct observation of heat dissipation in individual suspended carbon nanotubes using a two-laser technique. *J Appl Phys* 110:044328
143. Lin W, Shang J, Gu W, Wong CP (2012) Parametric study of intrinsic thermal transport in vertically aligned multi-walled carbon nanotubes using a laser flash technique. *Carbon* 50:1591–1603
144. Yue Y, Huang X, Wang X (2010) Thermal transport in multiwall carbon nanotube buckypapers. *Phys Lett A* 374:4144–4151
145. Shi L, Li DY, Yu CH, Jang WY, Kim D, Yao Z, Kim P, Majumdar A (2003) Measuring thermal and thermoelectric properties of one-dimensional nanostructures using a microfabricated device. *J Heat Transfer* 125:881–888
146. Yang J, Yang Y, Waltermire SW, Wu X, Zhang H, Gutu T, Jiang Y, Chen Y, Zinn AA, Prasher R, Xu TT, Li D (2012) Enhanced and switchable nanoscale thermal conduction due to van der Waals interfaces. *Nat Nanotechnol* 7:91–95
147. Colbourn EA (ed) (1994) *Computer simulation of polymers*. Longman, Harlow
148. Lee SW, Kim B-S, Chen S, Shao-Horn Y, Hammond PT (2009) Layer-by-layer assembly of all carbon nanotube ultrathin films for electrochemical applications. *J Am Chem Soc* 131:671–679
149. Yan XH, Xiao Y, Li ZM (2006) Effects of intertube coupling and tube chirality on thermal transport of carbon nanotubes. *J Appl Phys* 99:124305
150. Dresselhaus MS, Eklund PC (2000) Phonons in carbon nanotubes. *Adv Phys* 49:705–814
151. Zbib AA, Mesarovic SD, Lilleodden ET, McClain D, Jiao J, Bahr DF (2008) The coordinate buckling of carbon nanotube turfs under uniform compression. *Nanotechnology* 19:175704

152. Kim P, Shi L, Majumdar A, McEuen PL (2001) Thermal transport measurements of individual multiwalled nanotubes. *Phys Rev Lett* 87:215502
153. Wang S, Liang Z, Pham G, Park Y-B, Wang B, Zhang C, Kramer L, Funchess P (2007) Controlled nanostructure and high loading of single-walled carbon nanotubes reinforced polycarbonate composite. *Nanotechnology* 18:095708
154. Cao A, Dickrell PL, Sawyer WG, Ghasemi-Nejhad MN, Ajayan PM (2005) Super-compressible foamlike carbon nanotube films. *Science* 310:1307–1310